Available online at www.sciencedirect.com
SCIENCE DIRECT
Pattern Recognition 39 (2006) 646–668
PATTERN RECOGNITION
THE JOURNAL OF THE PATTERN RECOGNITION SOCIETY
www.elsevier.com/locate/patcog

Approaches for automated detection and classification of masses in mammograms

H.D. Cheng*, X.J. Shi, R. Min, L.M. Hu, X.P. Cai, H.N. Du

Department of Computer Science, 401B, Old Main Hall, Utah State University, Logan, UT 84322-4205, USA

Received 21 June 2004; accepted 12 July 2005

Abstract

Breast cancer continues to be a significant public health problem in the world. Early detection is the key for improving breast cancer prognosis. Mammography has been one of the most reliable methods for early detection of breast carcinomas. However, it is difficult for radiologists to provide both accurate and uniform evaluation for the enormous mammograms generated in widespread screening. The estimated sensitivity of radiologists in breast cancer screening is only about 75%, but the performance would be improved if they were prompted with the possible locations of abnormalities. Breast cancer CAD systems can provide such help and they are important and necessary for breast cancer control. Microcalcifications and masses are the two most important indicators of malignancy, and their automated detection is very valuable for early breast cancer diagnosis. Since masses are often indistinguishable from the surrounding parenchymal, automated mass detection and classification is even more challenging. This paper discusses the methods for mass detection and classification, and compares their advantages and drawbacks.
© 2005 Pattern Recognition Society. Published by Elsevier Ltd. All rights reserved.

Keywords: Mass; Mammogram; CAD; Wavelet; Fuzzy logic; Contrast enhancement; Feature selection

1. Introduction

Breast cancer happens to over 8% women during their lifetime, and is the leading cause of death of women in US [1]. Currently the most effective method for early detection and screening of breast cancers is mammography [2]. Microcalcifications and masses are two important early signs of the diseases [198]. It is more difficult to detect masses than microcalcifications because their features can be obscured or similar to normal breast parenchyma. Masses are quite subtle, and often occurred in the dense areas of the breast tissue, have smoother boundaries than microcalcifications, and have many shapes such as circumscribed, speculated (or stellate), lobulated or ill-defined. The circumscribed ones usually have a distinct boundaries, 2–30 mm in diameters, and are high-density radiopaque; the speculated ones have rough, star-shaped boundaries; and the lobulated ones have irregular shapes [3]. Masses must be classified as benign and malignant in order to improve the biopsy yield ratio. Generally speaking, masses with radiopaque and more irregular shapes are usually malignant, and those combined with radiolucent shapes are benign [117]. A mammogram is basically distinct with four levels of the intensities: background, fat tissue, breast parenchyma and calcifications with increasing intensity. Masses develop from the epithelial and connective tissues of breasts and their densities on mammograms blend with parenchyma patterns. Several studies have revealed a positive association of tissue type with breast cancer risks [4,5]. Women who have breast cancers can easily get contralateral cancers in the other side breast [6,7]. Distinguishing a new primary from metastasis was not always possible due to their similar features. Asymmetry of breast parenchyma between the two sides has been one of the most useful signs for detecting primary breast cancer [8].

* Corresponding author. Tel.: +1 435 797 2054; fax: +1 435 797 3265.
E-mail address: hengda.cheng@usu.edu (H.D. Cheng).

0031-3203/$30.00 © 2005 Pattern Recognition Society. Published by Elsevier Ltd. All rights reserved.
doi:10.1016/j.patcog.2005.07.006

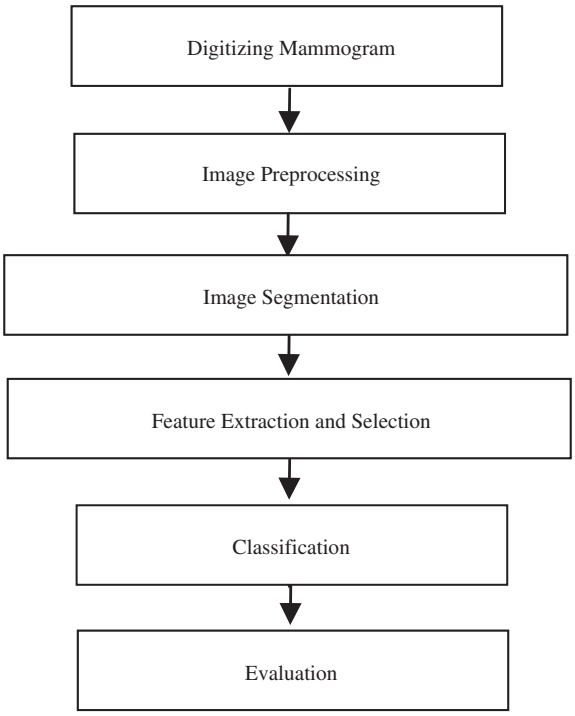

Fig. 1. CAD mass classification.

Reading mammograms is a very demanding job for radiologists. Their judgments depend on training, experience, and subjective criteria. Even well-trained experts may have an interobserve variation rate of 65–75% [9]. Computer aided diagnosis (CAD) systems may help radiologists in interpreting mammograms for mass detection and classification. Since 65–90% of the biopsies of suspected cancers turned out to be benign, it is very important to develop CADs that can distinguish benign and malignant lesions. The combination of CAD scheme and experts' knowledge would greatly improve the detection accuracy. The detection sensitivity without CAD is 80% and with CAD up to 90% [10]. Most of the mass detection CAD schemes involve the phases described in Fig. 1. First, image preprocessing of the digitized mammogram can suppress noise and improve the contrast of the image. Second, image segmentation is defined by most of the articles about mass detection as locating the suspicious regions. It is different from the common definition of segmentation in image processing. In the third phase, features are extracted and selected for classifying lesion types or removing false positives. Finally, the detection/classification of masses will be conducted. Although the CAD schemes were independently developed using different data sets of limited size, most of the schemes yielded similar performance, 85–95% true positive rate, with 1–2 false positives in an image. In this survey, the methods of five major research areas: preprocessing, image segmentation, feature extraction and selection, mass detection/classification, and performance evaluation will be studied.

2. Image preprocessing of mammograms

Preprocessing is an important issue in low-level image processing. The underlying principle of preprocessing is to enlarge the intensity difference between objects and background and to produce reliable representations of breast tissue structures. An effective method for mammogram enhancement must aim to enhance the texture and features of masses. The reasons are: (1) low-contrast of mammographic images; (2) hard to read masses in mammogram; (3) generally, variation of the intensities of the masses such that radiopaque mass with high-density and radiolucent mass with low-density in comparison with the background. The enhancement methods are grouped as: (1) global histogram modification approach; (2) local-processing approach; and (3) multiscale processing approach. The ideal contrast enhancement approach should enhance the mammograms with no over-enhancement and under-enhancement.

2.1. Global histogram modification approach

A commonly used global histogram modification approach is the histogram equalization (HE) [11]. The main idea is to re-assign the intensity values of pixels to make the new distribution of intensities uniform to the utmost extent. Suppose that $H(i)$ is the histogram of the image with size $M \times N$, and $[G_{\min}, G_{\max}]$ is the range of the intensities of the image. We can map the original image intensity I_{org} into the resulting image intensity I_{new} using HE technique as below:

$$I_{\text{new}} = G_{\min} + (G_{\max} - G_{\min}) \times \sum_{i=0}^{I_{\text{org}}} H(i)/(M \times N).$$

The HE technique is simple and effective in enhancing the entire image with low contrast, only if (a) it contains single object or (b) there is no apparent contrast change between the object and background. To improve HE method, Multi-peak HE method [85,179] has been developed. In this method, the range of the gray levels is $[x_0, x_L]$, one or more mid-nodes x_i $(i = 0, 1, \ldots)$ was determined by the values of mean, median or according to how many peaks are present in the histogram. Then the original histogram is partitioned into many pieces, and they are equalized piecewise and independently.

Another global histogram modification is the histogram stretching [11,12]. It uses a linear transfer function:

$$I_{\text{new}} = G_{\min} + (I_{\text{org}} - I_{\min}) \times (G_{\max} - G_{\min})/I_{\max} - I_{\min}),$$

where $[I_{\min}, I_{\max}]$ is the range of the intensities of the original image and $[G_{\min}, G_{\max}]$ is the range of intensities of the resulting image. The global histogram modifi-

Table 1
Methods based on wavelet transformations

Mother wavelets	Coefficient modification steps	Advantage/disadvantage
Dyadic wavelet [30–32,35–37]	1. An overcomplete multiscale representation is constructed 2. The separable and steerable filter is for detecting mass shape and locating orientation of texture pattern 3. The coherence at level i is defined, the "coherence maps" and orientation structures are adopted to capture distinct features at each level 4. Using the information obtained, a nonlinear operation was applied at each level to modify the transform coefficients and reconstruct the coefficients	It is the most popular wavelet and its scaling factor is a power of 2. It is good for horizontal and vertical features. The dyadic wavelet can cope with the lack of translation invariance and is useful for analyzing multiscale features
The cubic spline scaling wavelets [32]	1. Calculate the multiscale gradients of image 2. Detect the local gradient maxima at all scales 3. Modify the magnitude values of gradient maxima to get the wavelet transform of the enhanced image	It has the flexibility of selectively enhancing the features of different sizes and/or in different locations, and the capability of controlling noise magnification
Hexagonal wavelets [33,34,37,40,41]	Using nonlinear thresholding to modify wavelet coefficients	It has good orientation quality and more orientation selection. It has the flexibility of focusing on local features

Table 2
Enhancement methods

Method	Description	Advantage	Disadvantage
Global approach [11,12,85,179]	Re-assign the intensity values of pixels to make the new distribution of the intensities uniform to the utmost extent	Effective in enhancing the entire image with low contrast	1. Cannot enhance the textual information 2. Working only for the images having one object
Local approach [11,13–29]	Feature-based or using nonlinear mapping locally	Effective in local texture enhancement	Cannot enhance the entire image well
Multi-scale processing [30–38,40,41,189]	Based on wavelet transformation	Flexible to select local features to be enhanced, and able to suppress noise	Difficult to determine the mother wavelet and weight modification functions

cation almost has done nothing for texture enhancement since it cannot change the order of the gray levels of the original image, and it is not suitable for enhancing mammograms.

2.2. Local processing approach

Local-processing approaches are also studied for image contrast enhancement. There are many methods for contrast enhancement by changing pixel intensities. One way is based on nonlinear mapping methods (local histogram technique, bi-linear, sigmoid, non-continuous, etc.) [11,13–17]. The implementation can be feature-based, and the local features may be gained by edge detection, or by using local statistic information such as local mean, standard deviation, etc. The nonlinear mapping may be: (1) based on the gradient and/or local statistics, and the nonlinear functions [11–15,18–22]; or (2) adaptive histogram equalizations [15,23–25]. Another feature-based method is to define the contrast ratio first, then to enhance image contrast by increasing the contrast ratio [15,19,26–28] using an exponent function, etc. [29] proposed a multistage tree-structured filter to enhance the digital mammogram. Each stage is based on a central weighted median filter. The local-processing methods are quite effective in local texture enhancement. However, most of local methods have little contribution to enhancing the contrast among the objects. A technique combining the above methods is proposed in [12].

2.3. Multiscale processing approach

Some methods for feature enhancement are based on wavelet transformation [30–38,40,41,189]. The general stages can be described as: (1) The digitized mammogram is transformed using wavelets. (2) The coefficients are modified to enhance the mass features. (3) The enhanced mammogram is obtained using the inverse wavelet transformation.

The methods use the orientational information at each scale of the analysis. The differences of implementing this kind of methods are in the basis functions (or mother wavelets) and the ways to modify coefficients, as described in Table 1. It is flexible to select local features to be enhanced, and able to suppress noise. It can detect the directional features and remove unwanted perturbations. More orientational information is obtained using hexagonal sampling than rectangular sampling. However, it is difficult to decide what mother wavelet for transformation and what methods for modification to enhance all kinds of masses. The summary of the enhancement approaches is listed in Table 2.

3. Image segmentation

The second stage of mass detection CAD schemes is to separate the suspicious regions that may contain masses from the background parenchyma, i.e., to partition the mammogram into several non-overlapping regions, then extract regions of interests (ROIs), and locate the suspicious mass candidates from ROIs. The suspicious area is an area that is brighter than its surroundings, has almost uniform density, has a regular shape with varying size, and has fuzzy boundaries [18]. This is a very essential and important step that determines the sensitivity of the entire system. Segmentation methods do not need to be excruciating in finding mass locations but the result for segmentation is supposed to include the regions containing all masses even with some false positives (FP). FPs will be removed at a later stage. However, the result of a good segmentation depends on the suitable algorithm for the specific features, and if the algorithm is fixed, the result can be improved by the enhancement techniques [14]. According to their natures, there are four kinds of segmentation techniques: classical techniques, fuzzy techniques, bilateral image subtraction and multiscale technique. A summary of different segmentation techniques is described in Table 3.

Table 3
Segmentation techniques

Segmentation techniques and descriptions	Advantages and disadvantages	Refs.
Global thresholding: based on global information, such as the histogram of the mammograms	It is widely used; easy to implement; it is not good for identifying ROIs; and FNs and FPs may be too high	[39,42,43,46]
Local thresholding: the thresholding value is determined locally	It can refine the results of global thresholding, and is better for mass detection than global thresholding It cannot accurately separate the pixels into suitable sets. It is often used as an initialization of other algorithms	[44,45,47,48]
MRF/GRF (statistical methods): it uses the local neighborhood relationship to represent the global relationship	Good segmentation results; complex statistical computation, and time-consuming	[45,49–52,194]
Region growing: it finds a set of seed pixels first, then to grow iteratively and aggregate with the pixels that have similar properties	Refer to Table 4. The segmentation result depends on finding suitable seeds; and it may be sensitive to noise	[48,62–64]
Region clustering: searches the region directly without any prior information	It is similar to region growing (Refer Table 4). The k-means algorithm does not use the local spatial constraints; it assumes that each cluster has a constant intensity; and it needs to know the number of clusters	[71–77]
Edge detection: edge detection is a traditional method for image segmentation, and it detects the discontinuity in mammograms	Refer to Table 6 for the summary of the different edge detectors	[16,58,78–91]
Template matching: segments possible masses from the background using prototypes	Easy to implement; if the prototypes are appropriate, it can provide good results It depends on the prior information of the masses, it may result high number of false positives	[18,97,75,76,98,207]
Stochastic relaxation: an unsupervised with an evidential constrained optimization method	It is often used in a statistical model, and it builds an optimal label map to separate tissue and suspicious areas. Time-consuming and complex parameter estimation	[14,101,102]
Fuzzy technique: apply fuzzy operators, properties, and inference rules to deal with the uncertainty inherent in mammograms	The fuzzy techniques including fuzzy thresholding and fuzzy region clustering or growing; it can handle the unclear boundary between normal tissue and tumors; and it is not easy to determine the suitable membership functions and rules	[99,100,103–105]
Bilateral image subtraction: it is based on the normal symmetry between the left and right breasts	Easy to implement, and the difference between the left and right mammogram images can be identified as suspicious regions; it is difficult to register the left and right breasts correctly	[106–112,191]
Multiscale technique: apply DWT filters to transform the mammogram images from spatial domain to spatial frequency domain, and do further processing	Because of its ability to discriminate different frequencies/scales, it can preserve the resolution of the portion of ROI; it does not need any prior information; selecting suitable mother wavelets and weight modifying functions is not easy	[89,90,106,113–115]

3.1. Classical approaches

Roughly, the classical algorithms are divided into six subcategories: global thresholding, local thresholding, iterative pixel classification, edge detection, template matching and stochastic relaxation.

3.1.1. Global thresholding

Global thresholding has been widely used for segmentation [39,42,43,46]. The global thresholding technique is based on the global information, such as the histogram. Since the masses are brighter than the surrounding tissues, it makes thresholding a useful method for segmentation. The regions with abnormalities impose the extra peaks on histogram while a healthy region has only a single peak. After a global thresholding value is attained, the objects can be separated from the background. Methods depending only on the global thresholding are not good to identify ROIs. Because mammograms are the 2D projections of the 3D breasts, the regions of overlapping tissues including three kinds of tissues: a fat region, a fatty and glandular region and a dense region, may be brighter than the masses. The output of the global thresholding is mainly used as an input to the next step in most of systems.

3.1.2. Local thresholding

Local thresholding (LT) can refine the results of global thresholding or identify suspicious areas. LT is better for mass detection than global thresholding, because a local threshold value is determined locally for each pixel based on the intensity values of the surrounding pixels. Two variables of the local thresholding should be considered: the window size and thresholding value [47,48]. However, LT is a pixel-based operation and cannot accurately separate pixels into the suitable sets, and an adaptive clustering process is used to refine the result attained from the localized adaptive thresholding [44]. LT is also used as pre-processing for other algorithms, such as Markov random field [45].

3.1.3. Iterative pixel classification

There are three kinds of segmentation methods based on pixel classification: Markov random field (MRF) or Gibbs random field (GRF), region growing, and region clustering.

(1) *MRF/GRF*. The algorithms based on MRF/GRF for segmentation of mammograms have been studied [45,49–52,194]. MRFs/GRFs are statistical methods and powerful modeling tools [45,49–52]. A common criterion for MRF is to estimate a function of maximum a posteriori (MAP), i.e., to maximize the posterior distribution of the segmented image X,

$$X_{\mathrm{MAP}} = \arg\max_{x} \{p(X = x|Y = y)\}.$$

However, it is impractical to obtain the maximum value due to the high computational complexity. There are two categories of algorithms to estimate MAP functions: stochastic methods such as simulated annealing (SA), and deterministic methods such as iterated conditional modes (ICM) [45].

A modified Markov random field (MRF) model-based method was employed for segmenting mammogram images [45,49–52]. The algorithm uses the statistical properties of the pixel and its neighbors. The probability mass function $p_X(x)$ is defined as [52]

$$p_X(x) = \frac{1}{z} \exp\left(- \sum_{\{r,s\} \in C} \beta t(x_r, x_s) - \sum_{\{r\} \in C} \gamma_{x_r} \right),$$

where the texture class label X is an MRF with a four nearest neighborhood system, z is a normalized constant, C is the collection of cliques, β and γ_{x_r} are the parameters of MRF model, and

$$t(x_r, x_s) = \begin{cases} 1 & x_r = x_s, \\ 0 & \text{otherwise}, \end{cases}$$

Ref. [52] claimed that when $\beta = 2$, and if γ_{x_r} is suitably chosen, the algorithm will be reliable to classify pixels.

A method based on the discrete wavelet transform (DWT) and multiresolution Markov random field (MMRF) to segment the suspicious regions is studied [53–56]. They employed different wavelet mother functions. The expectation-maximization (EM) algorithm was used to evaluate the segmentation result [55,57]. The free-response receiver operating characteristic (FROC) curves to compare DWT with MRF methods was given in [58]. It claimed that the better results were obtained using DWT method than using MRF method.

Two statistical models based on the features of abnormalities are introduced [59]. In the Spatial Planar model, the background texture is characterized using a parametric model and the abnormalities were considered as the disturbance in the background texture and correspond to a low probability level. This approach suppressed the background texture while emphasizing the abnormalities. It finds the abnormalities with fewer false positives, but distorts the shapes detected. Another one is based on the Gibbs model, in which finding the abnormalities is considered as a statistical restoration of a noisy image. Both methods used joint probability distribution of an image to simultaneously estimate a smoothed version of the image and a binary image indicating the presence or absence of the abnormalities. They concluded that the abnormalities with few false positives were extracted when a spatial detector was applied, but the shapes of the detected objects were untrustworthy; while the shapes were better attained when GRF was applied.

(2) *Region growing*. Region growing is one of the popular techniques for segmenting masses in digitized mammograms. The basic idea of the algorithm is to find a set of seed pixels in the image first, and then to grow iteratively and aggregate with the pixels that have similar properties. If the region is not growing any more, then the grown region and surrounding region are obtained. Region growing may

Table 4
Region growing techniques

	Preprocessing	Advantage	Disadvantage	Refs.
Simple graphical seed-filling	1. Contrast stretching 2. Histogram equalization 3. Fixed-neighborhood statistical enhancement 4. Convolution mask enhancement 5. ANCE	Simple and easy to implement	Does not work well if no obvious peaks	[22,60,62,190]
Adaptive thresholding	1. Region partition 2. Automatic seed selection	Able to remove speckle noise	Very time-consuming	[63,64]
Probabilistic method and radial gradient index (RGI)-based method	A Gaussian function $h(x, y)=f(x, y)N(x, y; \mu_x, \mu_y, \sigma_c^2)$[a] to do lesion segmentation	If the mass region fits the Gaussian distribution, these two methods work well	Discrete contour model is better than this probabilistic method, RGI-based method is sensitive to noise	[65–68]
Adaptive region growing	1. Select an initial seed point 2. Define cutoff factor, mean and standard deviation 3. Define local window size	Reduce some noise	Very time-consuming	[66,69,70]

[a] $h(x, y)$ is the multiplication of the original ROI with the constraint function, $N(x, y; \mu_x, \mu_y, \sigma_c^2)$ is a circular normal distribution centered at (μ_x, μ_y) with variance σ_c^2.

Table 5
Comparison of region growing and region clustering

Algorithms	Region growing	Region clustering
Need a start point	Yes	No
Need prior information	Yes	No
Is an iterative process	Yes	Yes
Require update/stop function	Yes	Yes

be applied globally or locally. If the grown region of a seed has an average intensity greater than that of the surrounding, the region is classified as the parenchyma, or fat, tissue. The accuracy reaches 90% for classifying the tissue patterns [48]. The key issue of region growing is to find a criterion that checks whether the gray level values of its neighbors are within a specified deviation from the seed. The performance of the algorithm depends on the enhancement method, i.e., the algorithm will get a better result if a better enhancement method is applied. Adaptive neighborhood contrast enhancement (ANCE) method was applied to enhance the images before region growing [62]. Another key issue of region growing is to find the suitable seeds. An automatic seed selection was introduced [63]. There are three parts in mammograms: a fat region, a fatty and glandular region, and a dense region. According to the intensity values and local contrast between a seed pixel and its neighbors in the three partitions, three sets of seed pixels are selected from the partitioned regions. Then a region growing process was applied for segmentation [64]. The advantages/disadvantages of the methods based on region growing technique are summarized in Table 4.

(3) *Region clustering*. Region clustering and region growing are very similar. Region clustering searches the region directly without any prior information as described in Table 5.

The K-means algorithm is a well-known clustering procedure. An adaptive clustering algorithm for segmentation was introduced [71] to overcome two problems of the K-means algorithm: the lack of spatial constraints and the assumption of constant intensity in each cluster. The performance is better than K-means algorithm with/without spatial constraints, and better than region growing techniques. The adaptive clustering to refine the segmentation was also studied [44]. It employed the localized adaptive thresholding, a pixel-based operation, to partition a mammogram into two classes, and then for each pixel to update the segmentation and the confidence estimate based on the intensity values of its neighbors. A clustering algorithm was used for fully automated segmentation [72,73]. Similar to region growing technique, [74] used a pixel-by-pixel K-means clustering method [75–77] for initial mass segmentation. The clustering process separates one or more disjoint objects within the ROIs, which were filled, grown in a local neighborhood, and eroded and dilated by morphological operators.

3.1.4. Edge detection

Edge detection is a traditional method for image segmentation. There are a lot of operators, Roberts gradient, Sobel gradient [78], Prewitt gradient, Laplacian operator, etc. The combined edge detection method was developed in [79] to increase accuracy. A summary and comparison of different segmentation techniques is described in Table 6.

Table 6
Edge detection techniques

Edge detection techniques	Description	Refs.
DWCE	It is used in two stages, first applies it globally to isolate the suspected area, then uses it locally to refine the segmentation. It is in conjunction with LoG filter	[16,58,80,81]
Logic filter	It is a nonlinear filter, and logic operators AND, OR and *X*OR are used. The concrete logic expressions depend on the prior information, and the filter structure influences the results	[82–85]
Iris filter	It is an adaptive filter. It is applied locally	[86,87]
Gaussian filter	ROIs are highlighted by a DOG filter. It can reduce number of FPs	[88–90]
Deformable models	It is a contour or interface which after initialization moves according to its local properties and the priori information of the object. It is good in finding the contour of the suspected area. The performance may depend on the initialization	[65,68,92,93,95,201,202]

(1) *Density-weighted contrast enhancement (DWCE)*. The main purpose of the DWCE method is to enhance the structures within the mammogram to make the edge detection algorithm able to detect the boundaries of the objects [16]. DWCE filter in conjunction with Laplacian–Gaussian (LoG) filter for segmenting suspicious mass regions was studied [16,58,80]. DWCE was employed in two stages, first, globally to enhance the contrast and uses LoG to isolate the objects, and then locally to each of the segmented objects to refine the segmentation. Ref. [81] evaluated a modified DWCE in combination with a texture classification scheme.

(2) *Logic filter*. A nonlinear filter, logic filter, was introduced [82,83]. The logic operators of AND, OR and *X*OR are used, and the concrete logic expressions depend on applications. Label the window structure as the following,

$$\begin{matrix} a & b \\ c & [D] \end{matrix}$$

Here a, b, c, and D are four pixels and [ ] is the center of the structure. The logic filter is defined as

$$D = (D \ XOR \ b)OR(D \ XOR \ c)$$

A modified logic filter [84,85] detects the existence of the edge in all possible directions:

$$D = (D \ XOR \ a)OR(D \ XOR \ b)OR(D \ XOR \ c)$$

A median filter is employed before the logic filter to remove noise, and then a thresholding value is determined via the histogram to find the edge of the tumor. It successfully detected a test set of 25 sample mammograms [84]. However, the quality of the mammograms directly affects the results.

(3) *Iris filter*. An adaptive filter, iris filter, to extract ROIs in digital mammograms was studied [86,87]. After using the iris filter, the area of a tumor candidate is estimated by a simple thresholding, and then a snake algorithm (we introduce the snake algorithm in the following subsection) is employed to find the approximate boundary of the tumor candidate.

(4) *Gaussian filter*. A model-based vision (MBV) algorithm was used to obtain ROIs and classify the masses [88]. The targets of the algorithm are to reduce the rate of FPs, to extract the features from ROI's, and to match these features with those truth models. ROIs were highlighted by a difference of Gaussian (DoG) filter. DoG comes from Laplacian of the Gaussian (LoG), and because of computational reasons, LoG is implemented as DoG [89,90]. The DoG mask is as follows:

$$h(x, y) = \frac{1}{2\pi\sigma_1^2} e^{-(x^2+y^2)/2\sigma_1^2} - \frac{1}{2\pi\sigma_2^2} e^{-(x^2+y^2)/2\sigma_2^2}.$$

Applying Fourier transform to the above formula,

$$H(f_x, f_y) = e^{-\sqrt{2\pi}\sigma_1^2(f_x^2+f_y^2)} - e^{-\sqrt{2\pi}\sigma_{12}^2\left(f_x^2+f_y^2\right)}.$$

A good edge detector should satisfy the following conditions [91]: (1) low error probability of marking non-edge pixels and losing edge pixels; (2) edge pixels should be as near as possible to the real edge; (3) the boundary width should be one pixel.

(5) *Deformable models*. A deformable model is a contour or interface which after initialization moves according to its local properties, such as boundary, internal constrains, and also the priori information of the object [201]. The deformable models can be generally categorized as the implicit models and explicit models. They were introduced in [202]. The deformable models [94] attracted the attention due to its two dimensional model, snake, also known as "deformable contour model". Snake is good in finding the contours of the interested regions; it employs an energy minimization method to find the contour. The algorithm to improve the detection quality of the closed edges was introduced in [92]. A fast algorithm for finding active contours was developed in [93] that improved the active contour algorithm and saved the computational time. A discrete contour algorithm was studies in [68,95], which is fast and robust to detect the boundaries, and it was used for mass segmentation in mammograms [65]. The internal force is determined by the local shape and the goal is to minimize the local curvature. The high internal force makes the contours smooth. The external force is based on the image gradient magnitude. The

larger value of the external force yields more variable boundaries. Another contour model, the discrete dynamic contour model, which was used to discriminate malignant masses from normal tissue, was discussed in [96]. An implicit deformable model, Geodesic deformable models, is studied in [201].

The level set method was studied in [199], it is often used in the deformable model. The level set approach is widely used in medical image analysis [200]. To our knowledge, the level set is still not used for the segmentation of masses, however, it may be a good potential research topic.

3.1.5. Template matching

Template matching is one of the most common approaches for medical image segmentation. This method uses the prior information of mammograms, and segments possible masses from the background using the prototypes. The prototypes of possible masses are created based on the characteristics or physical features of the targeted masses [18,207], or based on the two-dimensional search function [97]. When the priori information about the size of the masses is not available, a range of sizes for the templates is used [1]. The matching criterion is measured by the least square technique [97] or by a cross correlation coefficient of the template [18,75]. The sub-regions that match the templates will produce high coefficients whereas the sub-regions that do not match will produce low coefficients. Incorporating additional pre-processing methods, it can make the process more efficient [76]. Template matching results in a large set of possible masses, a majority of which are FPs. The adaptive thresholding technique may fail to find suspicious masses with a partial loss, while Ref. [98] proposed a template matching algorithm that can solve the problem by using the similarity. The similarity was calculated for all ROIs with a partial loss to improve the performance of template matching.

3.1.6. Stochastic relaxation

An unsupervised segmentation method with an evidential constrained optimization method was studied [101]. It aimed to detect all different lesions. The method performs unsupervised partitioning to segment the image into homogenous regions by using 'generic labels'. It uses a constrained stochastic relaxation algorithm for building an optimal label map to separate tissues and suspicious areas. An evidential disparity function estimates the feature similarity of two blocks of pixels and realizes the partitioning.

A modified contextual Bayesian relaxation labeling (CBRL) algorithm was developed to segment possible masses [102]. The method creates a finite generalized Gaussian mixture (FGGM) probability density function using statistical modeling, and FGGM is a good model when the image features are unknown [14]. The expectation maximization (EM) algorithm is employed to estimate the FGGM model parameters. It performed pixel labeling using the CBRL algorithm. A statistical model based on a finite generalized Gaussian mixture was used to localize the possible mass areas using a stochastic relaxation labeling scheme. Abnormalities in the mammograms may be considered as the disturbance or noise to the background and their probability can be estimated.

Table 7
Results using bilateral image subtraction technique

Verified masses cases	TP masses detected in a set	Average suspected regions per image	
		Before feature analysis	After feature analysis
152	144 (95%)	21.4	11.0

3.2. Fuzzy technique

Because the contrast in mammograms is very low and the boundary between normal tissue and tumors is unclear, the traditional segmentation methods might not work well. Fuzzy logical has been introduced for segmenting suspicious masses [99]. The algorithm first assigns a fuzzy membership value to each pixel, and then an error value is calculated in iteration and the fuzzy membership is updated [100]. Effects of the neighboring pixels are also considered in the update rules. The algorithms stops when a zero error is reached, indicating that each pixel was assigned to either the bright or dark region, i.e., the mass region or background region. It has been proved that fuzzy set theory coupled with texture-based algorithms was very useful for the classification of masses [100]. There are basically two kinds of fuzzy methods: fuzzy thresholding and fuzzy region clustering or growing.

3.2.1. Fuzzy thresholding

Classical (global/local) thresholding techniques try to segment ROIs, but the techniques are only effective for the objects with clear boundaries. A few methods with fuzzy thresholding are proposed for solving this problem. A membership value is assigned for each pixel in an image by a fuzzy membership function, and then an iterative process is applied, the error value is calculated, and the fuzzy membership values are updated by an update rule [99,103].

3.2.2. Fuzzy region growing

Classical region growing technique tries to precisely define ROIs, but it is difficult to find a criterion because most malignant tumors with fuzzy boundaries extend from a dense core region to the surrounding tissues. The fuzzy approach is studied. Firstly, a fuzzy membership value for each pixel is defined by a fuzzy membership function; secondly, a starting point within the ROI is chosen; thirdly, an iterative process is executed: a few control parameters are computed, and the fuzzy membership values are updated; finally, after de-fuzzifying the membership values, the pixels with

the same value of the starting point consist of a ROI. This step guaranties the stability of the algorithm. It proposed a new concept of acceptance with restriction, and the algorithm is more stable than the classic region growing. Control parameters $\Delta\mu$ max, ΔCV max and β were employed [104,105]. Here the coefficient of variation (CoV) is defined as the standard deviation divided by the mean, i.e., $V=\sigma/\mu$. Their experiments show that fuzzy region growing can attain very good results for segmentation.

3.3. Bilateral image subtraction

The bilateral image subtraction technique [106–112,191] is used to determine the suspicious regions. It is also called the asymmetry approach [109,110]. It is based on the normal symmetry between the left and right breasts. The algorithm consists of the following steps:

(1) Alignment of the left and right breast images: first, the breast border and the nipple position are located. The registration procedure uses them to determine the relative spatial transforms to align the two breast images.

(2) Asymmetry detection: asymmetry between the left and right breast images is detected using bilateral image subtraction. First, pairs of the thresholded left and right images are obtained at various intensity levels. Second, the differences of each pair of images are detected using a subtraction of the left and right images. In the left and right breast images, the regions where the differences appeared in the subtracted image can be located as the suspicious regions. Many suspicious regions can be identified using the bilateral image subtraction technique. Some of them may not be true masses. To reduce the number of FPs, the feature-analysis techniques are needed. First, various features: the brightness, roughness, size, and shape of the suspicious region are considered. Then, the suspicious regions are classified using these features. Table 7 illustrates the results using bilateral image subtraction technique [106]. However, the source of the database was not given.

This technique can be used in an automated mass detection system, and can reduce the suspicious regions while the true positive regions are detected. But, there are two main disadvantages. First, the left and right breast mammograms are not always symmetry because of different image acquisition, orientation, and compression. Second, the asymmetry method cannot remove the FPs and classify the true positive regions into benign and malignant masses. It only provides the clues in extracting features for further processing.

3.4. Multiscale technique

Multiscale techniques were applied to segment the suspicious areas, and they can improve the detection rate. Tumors with the radii between 2 and 30 mm can be detected in different scales [89,90,106]. Discrete wavelet transform (DWT) is a powerful mathematical tool for image analysis, and DWT is one of the multiscale techniques. Adaptive and multi-scale processing for improving segmentation was studied [44]. It used DWT to decompose the features and used multi-scale representation to process mammograms, and then segmented ROIs with an adaptive method. Gradient operators were used to determine the line orientations. The shortcoming of the gradient operators for estimating the lines is that it cannot obtain the central part of the lines, and a multiscale line-based orientation map was applied to resolve this problem [89] and to detect stellate distortions in mammograms. [113] introduced a method based on wavelets for extracting the suspicious areas according to their shapes. [114,115] considered the shapes of suspicious areas were not enough for classification, and proposed a DWT method to analyze the contributing factors of the scale in the discriminating area shapes after these areas are extracted.

4. Feature extraction and selection

The third stage of mass detection by CAD (computer-aided diagnosis) schemes is the feature extraction and selection. The features can be calculated from the ROI characteristics such as the size, shape, density, and smoothness of borders, etc. [116]. The feature space is very large and complex due to the wide diversity of the normal tissues and the variety of the abnormalities. Only some of them are significant. Using excessive features may degrade the performance of the algorithm and increase the complexity of the classifier. Some redundant features should be removed to improve the performance of the classifier. Ref. [192] made an investigation of the feature-analysis techniques for extracting features from mammograms. [117] demonstrated that the performance of ANN (artificial neural network) and BBN (Bayesian belief network) can come to the same level in detecting masses with the same features from the same mammographic database. The feature extraction and selection is a key step in mass detection since the performance of CAD depends more on the optimization of the feature selection than the classification method.

Feature selection is the process of selecting an optimum subset of features from the enormous potential features available in a given problem domain after the image segmentation [103]. According to what features are selected, the feature space can be divided into three sub-spaces: intensity features, geometric features, and texture features. The typical features sorted by the sub-spaces are summarized in Table 8. The general guidelines to select significant features mainly include four considerations [118]: Discrimination, Reliability, Independence, and Optimality. The feature extraction and selection processes for mass detection can base on the principle component analysis [2], linear discriminate analysis [61,74], and GA algorithm [117,119,120]. [3]

proposed recursive functions to calculate the features and significantly reduced the complexity of the feature extraction. Some features that are not listed in the Table 8 were discussed in [122,123].

4.1. Intensity features

This kind of features is the simplest among the three subspaces, and most of them are the simple statistics [132]. The feature FI1 is the contrast measure of the suspicious region. Generally, it is the difference between the average gray level of the ROI and the average gray level of the surrounding region. The features FI2–FI5 are the statistics pertinent to the moments. FI6 is a set of features consisted of the third-order normalized Zernike moments [126].

4.2. Shape features

The shape features are also called the morphological or geometric features. These kinds of features are based on the shapes of ROIs. Almost twenty significant shape features are extracted in a variety of classifiers [70,118,124,129–131,133–139,141,142,193]. The first eleven features are directly calculated from the boundaries and areas of ROIs. Six of them are the statistics based on the distribution of the normalized radial length (NRL). The last four features are statistics based on the distribution of the normalized chord length (NCL). FG1 is obtained by applying the radial edge-gradient analysis technique within various neighborhoods of the grown regions to quantitate the margin speculation of a mass [137]. FG2 is the magnitude of the average gradient along the margin of the mass [124]. It can be used to evaluate the degree of the mass spiculation. The method to calculate the features FG3–FG8 is described [70]. FG9 has the ability to measure density variations across the boundaries of ROIs and can help to decide whether the tumor is benign or malignant [141]. FG10 is a shape factor independent of the pixel intensity [138,141]. FG11 is a set of seven features that are pertinent to the second- and third-order central invariant moments [138,141]. FG12 is based on the Fourier transform of the object boundary sequence [131]. The features FG13–FG18 are the statistics based on the normalized radial length (NRL) distribution. The radial length of a point on the tumor boundary is the Euclidean distance from this point to the mass centroid, whose co-ordinates are the average of the co-ordinates of all the points on the mass boundary. The NRL distribution is a set of data, each of which is normalized by dividing the maximum radial length. The mathematical definitions of these six features can be found in [70,135]. The features FG19–FG22 are the statistics based on the normalized chord length (NCL) distribution [138,141,174]. The definition of the NCL is similar to the NRL. The difference between them is the definition of the length. The chord length is defined as the Euclidean distance of a pair of points on the tumor boundary.

4.3. Textural features

The third feature subspace is based on the texture. All the features can be grouped into three classes based on what they are derived from: SGLD-based features, GLDS-based features, and RLS-based features. FT1–FT14 are based on the spatial gray level dependence (SGLD) matrices, or gray-level co-occurrence (GCM) matrices. SGLD matrices are used to measure the texture-context information. It is a 2-D histogram. An element of the SGLD matrix $P(i, j, d, \theta)$ is defined as the joint probability that the gray levels i and j occur separated by distanced d and along direction θ of the image. In order to simplify the computational complexity of the algorithm, the θ is often given as 0°, 45°, 90°, and 135°, and the distance d is often defined as the Manhattan or city block distance. The element $P(i, j, d, \theta)$ of the SGLD matrix can be expressed as

$$P(i, j, d, 0^\circ) = \|\{((x_1, y_1), (x_2, y_2)), |x_2 - x_1| = d, y_2 - y_1 = 0\}\|,$$

$$P(i, j, d, 45^\circ) = \|\{((x_1, y_1), (x_2, y_2)), (x_2 - x_1 = d, y_2 - y_1 = -d) \text{ or } (x_2 - x_1 = -d, y_2 - y_1 = d)\}\|,$$

$$P(i, j, d, 90^\circ) = \|\{((x_1, y_1), (x_2, y_2)), x_2 - x_1 = 0, |y_2 - y_1| = d\}\|,$$

$$P(i, j, d, 135^\circ) = \|\{((x_1, y_1), (x_2, y_2)), (x_2 - x_1 = d, y_2 - y_1 = d) \text{ or } (x_2 - x_1 = -d, y_2 - y_1 = -d)\}\|,$$

where $I(x, y)$ is the intensity value of the pixel at the position (x, y), $I(x_1, y_1) = i$, $I(x_2, y_2) = j$, and $\|S\|$ the number of the elements in the set S. Features FT1–FT14 can be extracted from the SGLD matrices with different distance d and direction θ. The image on which the SGLD matrices are calculated can be ROIs, or the rubber-band straightening transform (RBST) image of the ROIs. The RBST image is described in Fig. 2. It constructs a new image by transforming a band of pixels surrounding the mass onto the 2D spatial domain. Based on RBST image, two kinds of texture features were obtained [119,131,147]. The GLDS-based features FT15–FT18 [147,158] are extracted from the gray level difference statistics (GLDS) vector of an image [149]. The GLDS vector is the histogram of the absolute difference of pixel pairs separated by a given displacement vector $\delta = (\Delta x, \Delta y)$, where $I_\delta(x, y) = |I(x + \Delta x) - I(y + \Delta y)|$, and Δx and Δy are integers. An element of GLDS vector $p_\delta(i)$ can be computed by counting the number of times each

Table 8
The features

Sub-spaces	Feature descriptions
Intensity features	FI1: contrast measure of ROIs [70,118,121,124,128,129]; FI2: Average grey level of ROIs (Mean) [3,124,136]; FI3: standard derivation inside ROIs or variance [3,118,124,129,204]; FI4: skewness of ROIs [3]; FI5: kurtosis of ROIs [3]; FI6: A set of features composed of third-order normalized Zernike moments [125–127];
Shape features	FG1: Margin spiculation [124,136,137,142]; FG2: Margin sharpness [124,136,142]; FG3: Area measure [70,118,131,204]; FG4: Circularity measure [70,118,131,134,135,204]; FG5: Convexity [70,131]; FG6: Rectangularity [70,131]; FG7: perimeter [70,131]; FG8: Perimeter-to-area ratio [70,131,138,141]; FG9: Acutance measure [133,141]; FG10: A shape factor MF_{1-3} [138,141]; FG11: A set of seven low-order, central invariant moments[138,141]; FG12: Fourier descriptor [131,138,141]; *NRL features*: FG13: NRL boundary roughness [118,135]; FG14: NRL mean [70,118,129,131,134,135]; FG15: NRL entropy [70,131,134,135]; FG16: NRL area ratio [70,131,134,135]; FG17: NRL standard deviation [70,118,131,134,135]; FG18: NRL zero crossing count [70,131,134,135]; *NCL features*: FG19: NCL mean [138,141,174]; FG20: NCL variance [138,141,174]; FG21: NCL skewness [138,141,174]; FG22: NCL kurtosis [138,141,174];
Texture features	*SGLD features*: FT1: energy measure (OR angular second moment) [70,118,119,121,128,130,131,133,140,143–146]; FT2: correlation of co-occurrence matrix [70,118,119,121,128–131,133,140,143–147,158]; FT3: inertia of co-occurrence matrix [70,118,119,121,128,130,131,140,143,144,146]; FT4: entropy of co-occurrence matrix [70,119,121,128,130,131,133,140,143,144,146,147,158]; FT5: difference moment [118,119,121,130,133,144,146]; FT6: inverse difference moment [70,118,119,121,128,131,133,140,143,144,146]; FT7: sum average [70,118,119,128,130,131,140,143,144,146]; FT8: sum entropy [70,118,119,128,130,131,140,143,144,146]; FT9: difference entropy [70,118,119,128,130,131,140,143,144,146]; FT10: sum variance [70,128,131,143]; FT11: difference variance [70,128,131,143]; FT12: difference average [70,128,131,143]; FT13: information measure of correlation 1 [70,128,131,143]; FT14: information measure of correlation 2 [70,128,131,143]; *GLDS features*: FT15: contrast [147,148,158]; FT16: Angular second moment [147,148,158]; FT17: entropy [147,148,158]; FT18: mean [147,148,158]; *RLS features*: FT19: short runs emphasis [119,130,131,148]; FT20: long runs emphasis [119,130,131,148]; FT21: grey-level non-uniformity [119,130,131,148]; FT22: run length non-uniformity [119,130,131,148]; FT23: run percentage [119,130,131,148]

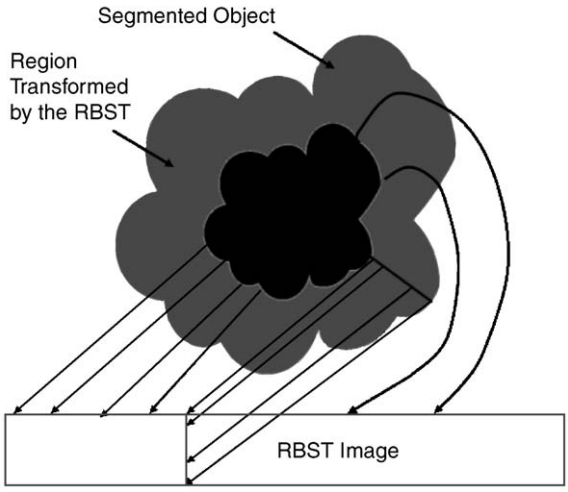

Fig. 2. The boundary pixels are mapped to the first row and the pixels on a normal line are mapped to a column of the RBST image [119].

value of $I_\delta(x, y)$ occurs. In practice, the displacement vector $\delta = (\Delta x, \Delta y)$ is usually selected to have a phase of value as 0°, 45°, 90°, or 135° to obtain the oriented texture features. The run length statistics (RLS) features FT19–FT22 of the RBST image are the inputs to the classifiers [119,131,142]. For a given image, it can compute a RLS matrix R_θ in a given direction θ [149]. A gray level run is a set of consecutive, collinear pixels with the same gray level value. The run length is the number of pixels in a given direction. The matrix element $R_\theta(i, j)$ represents the frequency of the run length j of gray level i in the direction θ.

4.4. Feature selection

Features extracted from the gray level characteristics, shape, and texture of the lesion and the surrounding tissue can usually be expressed as a mathematical description, and are helpful for a classifier to distinguish masses as malignant or benign. But, it is very difficult to predict which feature or feature combinations will achieve better classification rate. Generally, different feature combinations will result in different performance. In addition, relatively few features used in a classifier can keep the classification performance robust [150]. Therefore, one often faces with the task of selecting an optimized subset of features from a large number of available features. Two major methods for feature selection have been employed for CAD in mammography.

4.4.1. Stepwise feature selection

A common method to reduce the number of the features and obtain the best feature set is known as feature selection with stepwise linear discriminant analysis, or stepwise feature selection [76,77,119,140,151–155]. Stepwise feature selection is a heuristic procedure using statistical techniques based on Fisher's linear discriminant. At the beginning, the selected feature pool is empty. At each step followed, one available feature is input into or removed from the selected feature pool by analyzing its effect on a selection criterion. The discriminant analysis in the SPSS (Statistical Package for Social Sciences) software provides five selection criteria [151,155]: (1) the minimization of Wilks' lambda, (2) the minimization of unexplained variance, (3) the maximization of the between-class F statistic value, (4) the maximization of Mahalanobis distance, and (5) the maximization of Lawley-Hotelling trace. Most studies in mass detection [77,119,152–155] employed the minimization of Wilks' lambda as the selection criterion, which is defined as the ratio of within-group sum of squares to the total sum of squares [156]. Refs. [140,151] test all available selection criteria. A set of 340 features is reduced to 41 features with the stepwise feature selection [119].

4.4.2. Genetic algorithm (GA)

Another common method to select an optimized subset of features is genetic algorithms (GAs), which are adaptive heuristic search algorithms based on the principles of Darwinian evolution. In particular, GAs work very well on mixed combinatorial problems. However, they might be computationally expensive.

The possible solutions of the problem must be represented as chromosomes. The GA then creates a population of solutions based on the chromosomes and evolves the solutions by applying genetic operators such as mutation and crossover to find best solution(s) based on the predefined fitness function. The application of GA-based feature selection to mass detection has been studied [77,117,119,120,152,155,157]. The GA method with different fitness functions can reduce a set of 340 features to 39–62 features [119].

5. Classification

Once the features related to masses are extracted and selected, the features are input into a classifier to classify the detected suspicious areas into normal tissues, benign masses, or malignant masses. Classifiers such as the linear discriminants (LDA) and artificial neural network (ANN) have performed well in mass classification [76–78,80,81,117,118,120,147,158,159]. Tables 9 and 10 show the major classifiers and classifiers' combinations for mass classification.

5.1. Linear discriminant analysis (LDA)

LDA is a traditional method for classification [161,162]. The main idea of this method is to construct the decision boundaries directly by optimizing the error criterion to separate the classes of objects. If there are n classes, and linear discriminant analysis classifies the observations as the following n linear functions:

$$g_i(x) = W_i^{\mathrm{T}} \cdot x - c_i, \quad 1 \leqslant i \leqslant n,$$

Table 9
Classifiers for mass detection

Classifier	Description	Feature used	Advantage	Disadvantage
LDA [72,74,81,131,134,142,143,155]	Construct decision boundaries by optimizing certain criteria to classify cases into one of mutually exclusive classes	Texture features, shape features, morphological, and spiculation features	High performance for linear separable problem	Poor at adaptability, not online learning. Poor for non-linear separable data
(ANNs) [2,3,73,96,115,124,128,136,144,147,160,163–166,193,203–206,170]	Construct non-linear mapping function as a decision boundary. Two kinds of ANNs were used: the three-layer back-propagation neural network and the Radial Basis Function (RBF) network	Texture features, shape features, wavelet-based features, peak-related and contour-related features	Robustness, no rule or explicit expression is needed, widely applicable	No common rules to determine the size of ANNs, long training time, over training, not easy to explain why do they work
Bayesian network [78,117,120,168]	A probabilistic approach to estimate the class conditional probability density functions for background and tumor	50 local and four global features	Priori information can be easily incorporated into statistical models	Need to construct model and estimate the corresponding parameters
Binary decision tree [42,44,45,53,54,90]	A binary decision tree recursively using a threshold to separate mammogram data into two classes each time	Intensity features, shape features, texture features	Low complexity	Accuracy depends fully on the design of the decision tree and the features

Table 10
Classifier combinations for mass classification

Classifier combination	Description	Examples
Parallel architecture	All the classifiers are independent and their results are combined by a combiner	In [125,127], five different classifiers: multivariate Gaussian classifier (MVG), radial basis function (RBF), Q-vector median (QVM), 1-nearest neighbour (1NN) and hyperspheric Parzen windows (PZN) combine to detect the masses
Cascading architecture	All the classifiers invoke in a sequence. For efficiency, inaccurate but cheap classifiers are used first, followed by more accurate and expensive classifiers	In [80,81], a threshold classifier followed LDA and BPN classifiers. [153,154] proposed a new cascade classifier ART2LDA combining an unsupervised classifier ART2 and a supervised classifier based on LDA to improve classification performance
Hierarchical architecture	Individual classifiers are combined into a tree structure, and each node is associated with a classifier	In [42], the first level associated with deterministic classification and the area feature, and the rest three levels used Bayesian classifier and other types of features, such as shape descriptor, edge distance variation descriptor and edge intensity variation

where W_i^{T} is the transpose of a coefficient vector, x is a feature vector and c_i is a constant as the threshold. The values of W_i^{T} and c_i are determined through the analysis of a training set. Once the values of W_i^{T} and c_i are determined, they can be used to classify the new observations. The observation is abnormal if $g_i(x)$ is positive, otherwise it is normal. In [134], 60 mammographic masses were classified into three classes: stellate, nodular, and round by LDA. Seven traditional uniresolution shape features and three multiresolution shape features were used to classify with the result of 100% classification rate for the stellate masses, 70% for the nodular masses, and 80% for the round masses. By using the multiresolutional features, the overall classification rates were increased from 72% to 83%. In [74], a classifier using the stepwise feature selection and linear discriminant analysis was trained and tested on two sets of features (morphological and spiculation features) that were extracted using the machine segmentation and radiologist segmentation, respectively. The area A_Z under the ROC curve was 0.89 and 0.88, respectively.

5.2. Artificial neural networks (ANNs)

ANNs are the collection of mathematical models that imitate the properties of biological nervous system and the functions of adaptive biological learning. They are made of many processing elements that are highly interconnected together with the weighted links that are similar to the synapses. Unlike linear discriminants, ANNs usually use non-linear mapping functions as decision boundaries. The advantage of ANNs is their capability of self-learning, and often suitable to solve the problems that are too complex to use the conventional techniques, or hard to find algorithmic solutions.

It includes an input layer, an output layer and one or more hidden layers between them. Depending on the weight values of $w(j,i)$ and $w(k,j)$, the inputs are either amplified or weakened to obtain the solution in the best way. The weights are determined by training the ANN using the known samples. There are mainly two types of ANN classifiers for masses: the three-layer backpropagation neural network [2,144,163–166] and the radial basis function (RBF) network [2,3]. Generally, a known database of mammograms, including the selected features and the desire results, is selected to train the ANN. After the weights are determined, the ANN is ready to classify the masses. Ref. [2] used these two classifiers to classify 144 breast images from the MIAS database [http://www.wiau.man.ac.uk/services/MIAS/MIASmini.html]. They compared the results using different ANNs. The recognition rates are 65% using the RBF network, and 72% using the three-layer backpropagation neural network [2]. The average A_z value of 0.72 as the result of the three-layer backpropagation neural network is also better than 0.70 as the result of the RBF network.

5.3. Bayesian network

Bayesian network uses a probabilistic approach to determine an optimal classification for a given database. A BBN builds an "acyclic" graph in which the nodes represent the features variables, and connections between nodes represent direct probabilistic influences between the variables [167]. Each variable must have at least two discrete states and each state is associated with a probability value. For each node, the total of the probability values for all states equals 1. If there is no path between any two nodes, it indicates the probabilistic independence of two variables.

Bayesian classifier minimizes the total average loss [168]. A two-level hierarchical scheme consisting of Bayesian classifiers for each level is used to classify the masses [78]. The first level discriminates the speculated masses from the nonspiculated masses. The second level differentiates the masses with fuzzy areas from the masses with a well defined edge among the nonspiculated masses. In [117,120], a common database and the same genetic algorithm were used to optimize both the Bayesian belief network and neural network. The results show that the performance of the two techniques converged to the same level, hence, it concluded that the performance of CAD systems might be more dependent on feature selection and training database than on a particular classifier [117,120].

5.4. Binary decision tree

A binary decision tree recursively divides the feature space into two subspaces by selecting a threshold to separate input data into two classes each time. An ordered list of binary threshold operations on the features is organized as a tree. Each node has a threshold associating with one or more features to divide the data into its two descendents. The process stops when it only contains patterns of one class. Comparing with neural networks, the decision tree approach is much simpler and faster. In [53,54], after the mammogram was segmented into regions with different gray levels and features, a binary decision tree was used to classify the ROIs into the unsuspicious and suspicious classes.

Fuzzy logic can improve the performance of decision tree [44,45]. Fuzzy subset allows taking into account of membership that is useful to follow a different path for two values located on the both sides of the threshold of the test. A high value of the membership function will represent a high probability of the corresponding feature vector to be classified as a tumor. In [44,45], fuzzy binary decision tree was tested on a set of 100 normal images, 39 images with 48 minimal cancers and 25 images with 25 benign masses. The sensitivity TP = 93% with the false positive rate FP = 3.1 per image is obtained.

5.5. Combined classifiers

Sequential or parallel combinations of the classifiers are used to improve the classification rate. Each classifier may have its own region in the feature space where it performs the best. Many schemes for combining various classifiers have shown the classification accuracy is over that of individual classifier [169–171].

There are parallel, cascading and hierarchical types of classifier combinations [169]. In the parallel architecture, all the classifiers are independent and their results are combined by a combiner. In [125,127], five different classifiers such as multivariate Gaussian classifier (MVG), radial basis function (RBF), Q-vector median (QVM), 1-nearest neighbour (1NN) and hyperspheric Parzen windows (PZN) are combined to detect the circumscribed masses. The behavior–knowledge space (BKS) method is used to fuse all of the five classifiers. It is clear that the performance of the multi-classifier outperforms all of the individual classifiers. Tested on the data provided by the Kent and Canterbury Hospital NHS Trust in the UK, 95% of the masses are detected while keeping the false positive rate to a level comparable to that of individual classifiers with a much poorer true positive fraction (TPF) [125,127]. For the cascading architecture, all the classifiers invoke in a sequence. For the sake of efficiency, inaccurate but cheap classifiers are used first, followed by more accurate and expensive classifiers. [80,81] used a sequential classification scheme to reduce the number of FPs with the minimum number of TP losses. A threshold classifier simply sets a maximum and a minimum value for each morphological feature to prevent the followed LDA and BPN classifiers from training with non-representative features. The studies showed that the LDA and the BPN classifier were trained faster and performed better when the initial number of FPs in the training set was small, thus leading to the use of the sequential classification scheme [80,81]. By this method, FP = 4.4 per image at TP = 90% and FP = 2.3

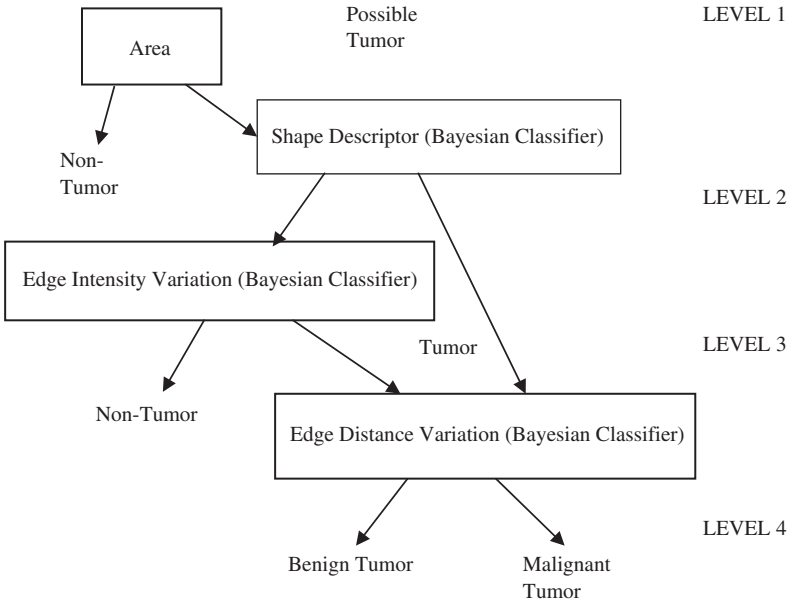

Fig. 3. A hierarchic classification example [42].

per image at TP = 80% are obtained. [153,154] proposed a new cascade classifier ART2LDA combining an unsupervised and a supervised classifier to improve the classification performance. The unsupervised model was based on an adaptive resonance theory (ART2) network [172,173] and the supervised model was based on LDA. The ART2LDA hybrid classifier is defined as

$$y = g\,(f_2(x))\,f_1(x) + 1 - g\,(f_2(x))$$

where x is the input feature vector, $f_1(\cdot)$ and $f_2(\cdot)$ are LDA and ART2 classifiers, respectively, and $g(\cdot)$ is a binary membership function defined as

$$g(c) = \begin{cases} 0 & \text{if } c \text{ is } a \text{ malignant class,} \\ 1 & \text{if } c \text{ is } a \text{ mixed class.} \end{cases}$$

Here, the mixed class contains both the malignant and benign members, while the malignant class only contains the malignant members. ART as an unsupervised classifier is first used to analyze the similarities of the input feature vector and eliminate a subpopulation that may be separated from the main population. This improves the performance of the second-stage LDA because the remaining population is more like multivariate normal distribution for which LDA is an optimal classifier. In the hierarchical architecture, individual classifiers are combined into a tree structure. Each tree node is associated with a classifier. This architecture has high efficiency and flexibility to discriminate different types of features. The classification hierarchy in [42] used the deterministic or Bayesian classifiers with four features to perform classification. The four features were the area of an extracted region, shape descriptor, edge distance variation descriptor and edge intensity variation. The first level associated with the deterministic classification and the area feature, and the other three levels used the Bayesian classifier and the rest three types of the features respectively (Fig. 3).

6. Evaluation of CAD performance

It is important to notice that an objective comparison of the performance of different CAD methods is very difficult and even impossible due to the use of different databases. Not only the cases of the different databases are different but also the proportion of subtle cases versus obvious cases is different. Even if a common database is used to test different methods, it could not guarantee that the comparison is valid and just. In Table 11 we list several available mammogram databases. In addition to the databases, the methods of evaluation will also influence the performance of the computer-aided diagnosis systems. Next, we will summarize various performance indices for the evaluation of CAD systems.

A receiver operating characteristic (ROC) curve is a plotting of true positive as a function of false positive [180–184]. Higher ROC, approaching the perfection at the upper left hand corner, would indicate greater discrimination capacity. The CLABROC program tests the statistical significance of the difference between two ROC curves [184]. For evaluating true-positive detection, sometimes it is required not only the existence but also the localization of the tumor. A better method for this purpose is the free-response receiver operating characteristic (FROC) analysis which is a plot of the operating points showing the tradeoff between the TP rate versus the average number of false positives per

Table 11
Available mammogram databases [175]

Database name	Description
DDSM	Digital database for screening mammography was created by Massachusetts General Hospital, the University of South Florida, and Sandia National Laboratories Source: http://marathon.csee.usf.edu/Mammography/Database.html
LLNL/UCSF	Database was created by Lawrence Livermore National Laboratories (LLNL) and the Radiology Department at the University of California at San Francisco (UCSF) Source: mammo-db-help@llnl.gov
MIAS	Database was created by the Mammographic Image Analysis Society (MIAS), United Kingdom Source: http://www.wiau.man.ac.uk/services/MIAS/MIASweb.html mias@svl.smb.man.ac.uk
Nijmegen	Database was created by the National Expert and Training Centre for Breast Cancer Screening and the Department of Radiology at the University of Nijmegen, the Netherlands Source: nico@mbfys.kun.nl

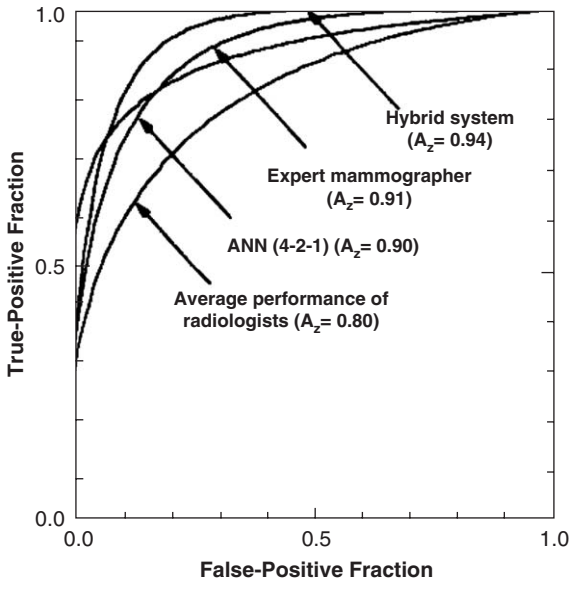

Fig. 4. ROC curves illustrate the performances of different systems to differentiate between benign and malignant masses [124].

image [176,185–187]. However, both FROC and ROC analyses suffer from their limitations. For instance, they do not address the complexity of the images and are difficult to transform the subjective measurements (radiologist's observations) to the objective FROC/ROC curves. The area under the ROC curve or the FROC curve is an important criterion for evaluating the diagnostic performance [176,177]. Usually, it is referred as the A_Z index. The A_Z value of ROC curve is just the area under the ROC curve. The A_Z value of FROC curve should be computed by normalizing the area under the FROC curve by the range of the abscissa. The value of A_Z is 1.0 when the diagnostic detection has perfect performance which means that TP rate is 100% and FP rate is 0%. The ROCFIT program [188] is for estimating A_Z from the ROC experiment. The estimation of the A_Z value can be obtained with the trapezoidal rule which can underestimate areas under the curve. More operating points are generated, less underestimation error will be obtained. The A_Z value can also be computed by fitting a continuous binomial curve to the operating points, provided the functional equation of the ROC curve is given [178].

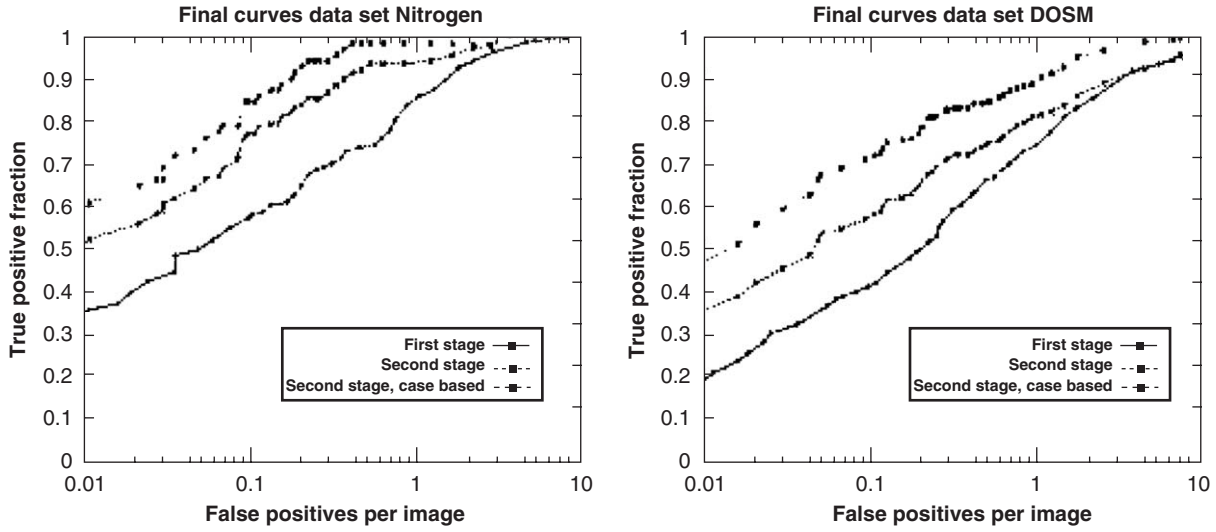

Fig. 5. FROC curves for the data sets from Nijmegen (left) and the DDSM (right) [96].

Fig. 4 shows ROC curves of an experienced radiologist, the average performance of five radiologists, the computerized scheme with ANN alone, and computerized the hybrid system [124]. $A_Z s$ were also calculated to evaluate the ability of different classifiers. The performance of the hybrid system with $A_Z = 0.94$ is better than all the others'. The experienced radiologist had an A_Z of 0.91, whereas the average of the five radiologists yielded an A_Z of 0.81. The four-input ANN yielded an A_Z value of 0.90. An example of the use of FROC curves for mass detection on two different data sets is given in Fig. 5 [96]. To measure the performance of the final result, an index A_f similar to index A_Z was defined as the area under the logarithmically plotted FROC curves between 0.05 and 4 FPs per image. A sensitivity level over 70% on the Nijmegen data set was achieved at a specificity of one FP in 10 images, whereas only 55% of the masses were found at a specificity level of one false positive per 10 images on the DDSM data set, which shows the differences in screening practice between the Netherlands and the USA.

Currently, breast ultrasound imaging becomes an important adjunct to mammography in mass detection [195–197], however, it will not be discussed here.

References

[1] A.S. Constantinidis, M.C. Fairhurst, F. Deravi, M. Hanson, C.P. Wells, C. Chapman-Jones, Evaluating classification strategies for detection of circumscribed masses in digital mammograms, in: Proceedings of 7th International Conference on Image Processing and its Applications, 1999, pp. 435–439.

[2] K. Bovis, S. Singh, J. Fieldsend, C. Pinder, Identification of masses in digital mammograms with MLP and RBF nets, in: Proceedings of the IEEE-INNS-ENNS International Joint Conference on Neural Networks Com, 2000, pp. 342–347.

[3] I. Christoyianni, E. Dermatas, G. Kokkinakis, Fast detection of masses in computer-aided mammography, IEEE Signal Process. Mag. 17 (1) (2000) 54–64.

[4] R.L. Egan, R.C. Mosteller, Breast cancer mammography patterns, Cancer 40 (1977) 2087–2090.

[5] J.N. Wolfe, Breast patterns as an index of risk for developing breast cancer, Am. J. Roentgen. 126 (1976) 1130–1139.

[6] H.H. Storm, O.M. Jensen, Risk of contralateral breast cancer in Denmark 1943-80, Br. J. Cancer 54 (1986) 483–492.

[7] G.F. Robbins, J.W. Berg, Bilateral primary breast cancers, A Prospective Clinicopathol. Study Cancer 17 (1964) 1501–1527.

[8] T.J. Rissanen, H.P. Makarainen, M.A. Apaja-Sarkkinen, E.L. Lindholm, Mammography and ultrasound in the diagnosis of contralateral breast cancer, Acta Radiol. 36 (1995) 358–366.

[9] P. Skaane, K. Engedal, A. Skjennald, Interobserver variation in the interpretation of breast imaging, Acta Radiol. 38 (1997) 497–502.

[10] K. Doi, Computer-aided diagnosis: potential usefulness in diagnostic radiology and telemedicine, in: Proceedings of National Forum '95, 1996, pp. 9–13.

[11] S.H. Nam, J.Y. Choi, A method of image enhancement and fractal dimension for detection of microcalcifications in mammogram, in: Proceedings of the 20th Annual International Conference of the IEEE Engineering in Medicine and Biology Society 20, vol. 2, 1998, pp. 1009–1012.

[12] M. Wilson, R. Hargrave, S. Mitra, Y.Y. Shieh, G.H. Roberson, Automated detection of microcalcifications in mammograms through application of image pixel remapping and statistical filter, in: Proceedings of the IEEE Symposium on Computer-based Medical Systems, 1998, pp. 270–274.

[13] J.K. Kim, J.M. Park, K.S. Song, H.W. Park, Adaptive mammographic image enhancement using first derivative and local statistics, IEEE Trans. Med. Imaging 16 (5) (1997) 495–502.

[14] H. Li, K. Liu, Y. Wang, S.C. Lo, Nonlinear filtering enhancement and histogram modeling segmentation of masses for digital mammograms, The IEEE 18th Annual International Conference on Bridging Disciplines for BioMedicine, vol. 3, 1997, pp. 1045–1046.

[15] D. Braccialarghw, G.H. Kaufmann, Contrast enhancement of mammographic features: a comparison of four methods, Opt. Eng. 35 (1) (1996) 76–80.

[16] N. Petrick, H.P. Chan, B. Sahiner, D. Wei, An adaptive density-weighted contrast enhancement filter for mammographic breast mass detection, IEEE Trans. Med. Imaging 15 (1) (1996) 59–67.

[17] K. Woods, L.P. Clarke, R. Welthuizen, Enhancement of digitized mammograms using a local thresholding technique, Annual International Conference of the IEEE Engineering in Medicine and Biology Society 13, vol. 1, 1991, pp. 114–115.

[18] S.M. Lai, X. Li, W.F. Biscof, On techniques for detecting circumscribed masses in mammograms, IEEE Trans. Med. Imaging l8 (4) (1989) 377–386.

[19] R. Gordon, R.M. Rangayyan, Feature enhancement of film mammograms using fixed and adaptive neighborhoods, Appl. Opt. 23 (4) (1984) 560–564.

[20] A.P. Dhawan, G. Buelloni, R. Gordon, Enhancement of mammographic features by optimal adaptive image processing, IEEE Trans. Med. Imaging 5 (1) (1986) 8–16.

[21] P.G. Tahoces, J. Correa, M. Souto, C. Gonzalez, L. Gonez, J.J. Vidal, Enhancement of chest and breast radiographs by automatic spatial filtering, IEEE Trans. Med. Imaging 10 (3) (1991) 330–335.

[22] S. Singh, R. Al-Mansoori, Identification of regions of interest in digital mammograms, J. Intell. Systems 10 (2) (2000) 183–210.

[23] J.P. Ericksen, S.M. pizer, J.D. Austin, MAHEM: a multiprocessor engine for fast contrast limited adaptive histogram equalization, Med. Imaging IV: Imaging Process. Proc. SPIE 1233 (1990) 322–333.

[24] K. Rehm, G.W. Seeley, W.J. Dallas, T.W. Ovitt, J.F. Seeger, Design and testing of artifact-suppressed adaptive histogram equalization: a contrast-enhancement technique for display of digital chest radiographs, J. Thorac. Imaging 5 (1990) 85–91.

[25] E.D. Pisano, S. Zong, B.M. Hemminger, M. DeLuca, R.E. Johnston, K. Muller, M.P. Braeuning, S.M. Pizer, Contrast limited adaptive histogram equalization image processing to improve the detection of simulated spiculations in dense mammograms, J. Digital Imaging 11 (4) (1998) 193–200.

[26] Y. Xiong, C.F. Lam, G.D. Frey, M.R. Croley, Contrast enhancement of mammogram by image processing, SPIE 1898 Image Process. (1993) 852–858.

[27] A.P. Dhawan, E. Le Royer, Mammographic feature enhancement by computerized image processing, Comput. Methods Programs BioMed. 27 (1988) 23–35.

[28] J.F. Urias, Feature enhancement of images using maximal contrast pixel to pixel, Appl. Opt. 30 (1991) 4598–4599.

[29] W. Qian, L.P. Clarke, M. Kallergi, R.A. Clark, Tree-structured nonlinear filters in digital mammography, IEEE Trans. Med. Imaging 13 (1) (1994) 25–36.

[30] C.M. Chang, A. Laine, Enhancement of mammograms from oriented information, in: IEEE International Conference on Image Processing, 1997, pp. 524–527.

[31] S. Mallat, S. Zhong, Characterization of signals from multiscale edges, IEEE Trans. Pattern Anal. Mach. Intell. 14 (7) (1992) 710–732.

[32] J. Lu, D.M. Healy, J.B. Weaver, Contrast enhancement of medical images using multiscale edge representation, Opt. Eng. 33 (7) (1994) 2151–2161.

[33] R.S. Pfisterer, F. Aghdasi, Hexagonal wavelets for the detection of masses in digitised mammograms, in: Proceedings of SPIE—The International Society for Optical Engineering, vol. 3813, 1999, pp. 966–977.
[34] R. Pfisterer, F. Aghdasi, Detection of masses in digitized mammograms, in: Proceedings of the South African Symposium on Communications and Signal Processing, COMSIG, Los Alamitos, CA, USA, 1998, pp. 115–120.
[35] C.M. Chang, A. Laine, Coherence of multiscale features for enhancement of digital mammograms, IEEE Trans. Inform. Technol. BioMed. 3 (1) (1999) 32–46.
[36] A. Laine, J. Fan, W. Yang, Wavelets for contrast enhancement of digital mammography, IEEE Eng. Med. Biol. 14 (5) (1995) 536–550.
[37] A.F. Laine, S. Schuler, J. Fan, W. Huda, Mammographic feature enhancement by multiscale analysis, IEEE Trans. Med. Imaging 13 (4) (1994).
[38] W. Qian, L. Li, L.P. Clarke, F. Mao, R.A. Clark, Adaptive CAD modules for mass detection in digital mammography, in: Proceeding of the 20th Annual International Conference of the IEEE Engineering in Medicine and Biology Society 20, vol. 2, 1998.
[39] V. Gimenez, D. Manrique, J. Rios, A. Vilarrasa, Iterative method for automatic detection of masses in digital mammograms for computer-aided diagnosis, in: Proceedings of SPIE—The International Society for Optical Engineering 3661, vol. II, 1999, pp. 1086–1093.
[40] R. Pfisterer, F. Aghdasi, Tumor detection in digitized mammograms by image texture analysis, Opt. Eng. 40 (2) (2001) 209–216.
[41] R. Pfisterer, F. Aghdasi, Comparison of texture based algorithms for the detection of masses in digitized mammograms, Africon, ISBN: 0-7803-5546-6, 1999, pp. 383–388.
[42] D. Brzakovic, X.M. Luo, P. Brzakovic, An approach to automated detection of tumors in mammograms, IEEE Trans. Med. Imaging 9 (3) (1990) 233–241.
[43] T. Matsubara, H. Fujita, S. Kasai, M. Goto, Y. Tani, T. Hara, T. Endo, Development of new schemes for detection and analysis of mammographic masses, Intel. Inform. Systems (1997) 63–66.
[44] L.H. Li, W. Qian, L.P. Clarke, R.A. Clark, J. Thomas, Improving mass detection by adaptive and multi-scale processing in digitized mammograms, in: Proceedings of SPIE—The International Society for Optical Engineering 3661, vol. 1, 1999, pp. 490–498.
[45] H.D. Li, M. Kallergi, L.P. Clarke, V.K. Jain, R.A. Clark, Markov random field for tumor detection in digital mammography, IEEE Trans. Med. Imaging 14 (3) (1995) 565–576.
[46] M. Abdel-Mottaleb, C.S. Carman, C.R. Hill, S. Vafai, Locating the boundary between breast skin edge and the background in digitized mammograms, in: K. Doi, M.L. Giger, R.M. Nishikawa, R.A. Schmidt (Eds.), Digital Mammography, Elsevier, Amsterdam, 1996, pp. 467–470.
[47] R.C. Gonzalez, P. Wintz, Digital Image Processing, Addison-Wesley Publishing Company, New York, 1992.
[48] M. Kallergi, K. Woods, L.P. Clarke, W. Qian, R.A. Clark, Image segmentation in digital mammography: comparison of local thresholding and region growing algorithms, Comput. Med. Imaging Graph. 16 (5) (1992) 231–323.
[49] S. Geman, D. Geman, Stochastic relaxation, Gibbs distributions, and Bayesian restoration of images, IEEE Trans. Pattern Anal. Mach. Intel. PAMI-6 (1984) 721–741.
[50] H. Derin, H. Elliott, Modeling and segmentation of noisy and textured images using Gibbs random fields, IEEE Trans. Pattern Anal. Mach. Intel. PAMI-9 (1) (1987) 39–55.
[51] J.T. Tou, R.C. Gonzalez, Pattern Recognition Principles, Addison-Wesley, Reading, MA, 1974.
[52] M.L. Comer, S. Liu, E.J. Delp, Statistical segmentation of mammograms, in: K. Doi, M.L. Giger, R.M. Nishikawa, R.A. Schmidt (Eds.), Digital Mammography, Elsevier, Amsterdam, 1996, pp. 475–478.
[53] L. Zhen, A.K. Chan, An artificial intelligent algorithm for tumor detection in screening mammogram, IEEE Trans. Med. Imaging 20 (7) (2001) 559–567.
[54] L. Zheng, A.K. Chan, G. McCord, S. Wu, J.S. Liu, Detection of cancerous masses for screening mammography using discrete wavelet transform-based multiresolution Markov random field, J. Digital Imaging 12 (2,1) (1999) 18–23.
[55] C.H. Chen, G.G. Lee, Image segmentation using multiresolution wavelet analysis and expectation-maximization (EM) algorithm for digital mammography, Int. J. Imaging Systems Technol. 8 (5) (1997) 491–504.
[56] C.H. Chen, G.G. Lee, A multiresolution wavelet analysis of digital mammograms, Proceedings of the 13th International Conference on Pattern Recognition, vol. 2, 1996, pp. 710–714.
[57] C.H. Chen, G.G. Lee, On digital mammogram segmentation and microcalcification detection using multiresolution wavelet analysis, Graph. Models Image Process. 59 (5) (1997) 349–364.
[58] L.H. Li, W. Qian, L.P. Clarke, Digital mammography: computer-assisted diagnosis method for mass detection with multiorientation and multiresolution wavelet transforms, Acad. Radiol. 4 (1997) 724–731.
[59] B. Calder, S. Clarke, L. Linnett, D. Carmichael, Statistical models for the detection of abnormalities in digital mammography, IEE Colloquium on Digital Mammography, London, UK, 1996, pp. 6/1–6/6.
[60] W.M. Morrow, R.B. Paranjape, Region-based contrast enhancement of mammograms, IEEE Trans. Med. Imaging 11 (3) (1992) 392–406.
[61] Z. Huo, M.L. Giger, C.J. Vyborny, F.I. Olopade, D.E. Wolverton, Computer-aided diagnosis: analysis of mammographic parenchyma patterns and classification of masses on digitized mammograms, in: Proceedings of the 20th Annual International Conference of the IEEE Engineering in Medicine and Biology Society, vol. 20, No. 2, 1998, pp. 1017–1020.
[62] R.M. Rangayyan, L. Shen, Y. Shen, J.E.L. Desautels, H. Bryant, T.J. Terry, N. Horeczko, M.S. Rose, Improvement of sensitivity of breast cancer diagnosis with adaptive neighborhood contrast enhancement of mammograms, IEEE Trans. Inform. Technol. BioMed. 1 (3) (1997) 161–170.
[63] Y.J. Lee, J.M. Park, H.W. Park, Mammographic mass detection by adaptive thresholding and region growing, Int. J. Imaging Systems Technol. 11 (5) (2000) 340–346.
[64] S.A. Hojjatoleslami, J. Kittler, Region growing: a new approach, IEEE Trans. Image Process. 7 (7) (1998) 1079–1084.
[65] G.M. Brake, M.J. Stoutjesdijk, N. Karssemeijer, A discrete dynamic contour model for mass segmentation in digital mammograms, in: Proceedings of SPIE—The International Society for Optical Engineering, Bellingham, WA, USA, vol. 3661, No. 2, 1999, pp. 911–919.
[66] M.A. Kupinski, M.L. Giger, Automated seeded lesion segmentation on digital mammograms, IEEE Trans. Med. Imaging 17 (4) (1998) 510–517.
[67] U. Bick, M.L. Giger, R.A. Schmidt, K. Doi, A new single-image method for computer-aided detection of small mammographic masses, in: Proceedings of CAR 95: International Symposium of Computer and Communication Systems for Image Guided Diagnosis and Therapy, 1995, pp. 357–363.
[68] G.M. Brake, N. Karssemeijer, Segmentation of suspicious densities, Med. Phys. 28 (2) (2001) 258–266.
[69] S. Pohlman, K.A. Powell, N.A. Obuchowski, W.A. Chilcote, S. Grundfest-Broniatowski, Quantitative classification of breast tumors in digitized mammograms, Med. Phys. 23 (1996) 1337–1345.
[70] N. Petrick, H.P. Chan, B. Sahiner, M.A. Helvie, Combined adaptive enhancement and region-growing segmentation of breast masses on digitized mammograms, Med. Phys. 26 (1999) 1642–1654.
[71] T.N. Pappas, An adaptive clustering algorithm for image segmentation, IEEE Trans. Signal Process. 40 (2) (1992) 901–914.

[72] B. Sahiner, H.P. Chan, N. Petrick, M.A. Helvie, M.M. Goodsitt, D.D. Adler, Classification of masses on mammograms using a rubber-band straightening transform and feature analysis, Proceedings of SPIE—The International Society for Optical Engineering, vol. 2710, 1996, pp. 44–50.
[73] B. Sahiner, H.P. Chan, N. Petrick, M.A. Helvie, M.M. Goodsitt, Computerized classification of benign and malignant masses on digitized mammograms: a study of robustness, Acad. Radiol. 7 (2000) 1077–1084.
[74] B. Sahiner, N. Petrick, H.P. Chan, Computer-aided characterization of mammographic masses: accuracy of mass segmentation and its effects on characterization, IEEE Trans. Med. Imaging 20 (12) (2001) 1275–1284.
[75] S.L. Ng, W.F. Bischof, Automated detection and classification of breast tumors, Comput. Biomed. Res. 25 (1992) 218–237.
[76] F.N. Che, M.C. Fairhurst, C.P. Wells, M. Hanson, Evaluation of a two-stage model for detection of abnormalities in digital mammograms, in: Proceedings of the 1996 IEE Colloquium on Digital Mammography, No. 072, London, UK, 1996.
[77] B. Sahiner, H.P. Chan, N. Petrick, D. Wei, M.A. Helvie, D.D. Adler, M.M. Goodsitt, Image feature selection by a genetic algorithm: application to classification of mass and normal breast tissue on mammograms, Med. Phys. 23 (1996) 1671–1684.
[78] J.L. Viton, M. Rasigni, G. Rasigni, A. Liebaria, Method for characterizing masses in digital mammograms, Opt. Eng. 35 (12) (1996) 3453–3459.
[79] M. Abdel-Mottaleb, C.S. Carman, C.R. Hill, S. Vafai, Locating the boundary between the breast skin edge and the background in digitized mammograms, in: K. Doi, M.L. Giger, R.M. Nishikawa, R.A. Schmidt (Eds.), Digital Mammography, Elsevier, Amsterdam, 1996, pp. 467–470.
[80] N. Petrick, H.P. Chan, B. Sahiner, D. Wei, M.A. Helvie, M.M. Goodsitt, D.D. Adler, Automated detection of breast masses on digital mammograms using adaptive density-weighted contrast enhancement filtering, Proceedings of SPIE—The International Society for Optical Engineering, vol. 2434, 1995, pp. 590–597.
[81] N. Petrick, H.P. Chan, D. Wei, B. Sahiner, M.A. Helvie, D.D. Adler, Automated detection of breast masses on mammograms using adaptive contrast enhancement and texture classification, Med. Phys. 23 (10) (1996) 1685–1696.
[82] K. Tsirikolias, B.G. Mertzios, Logic filters in image processing, in: Proceedings of the International Conference on Digital Signal Processing, Florence, Italy, September 4–6, 1991, pp. 285–287.
[83] K. Tsirikolias, B.G. Mertzios, Edge extraction and enhancement using coordinate logic filters, Image Process.: Theory Appl. (1993) 251–254.
[84] A. Rocha, F. Tong, Z.Z. Yan, Logic filter for tumor detection on mammograms, J. Comput. Sci. Technol. 15 (6) (2000) 629–632.
[85] K. Wongsritong, K. Kittayaruasiriwat, F. Cheevasuvit, K. Dejhan, A. Somboonkaew, Contrast enhancement using multipeak histogram equalization with brightness preserving, in: IEEE Asia-Pacific Conference on Circuits and Systems—Proceedings, 1998, pp. 455–458.
[86] H. Kobatake, Y. Yoshinaga, Detection of spicules on mammogram based on skeleton analysis, IEEE Trans. Med. Imaging 15 (3) (1996) 235–245.
[87] H. Kobatake, M. Murakami, H. Takeo, S. Nawano, Computerized detection of malignant tumors on digital mammograms, IEEE Trans. Med. Imaging 18 (5) (1999) 369–378.
[88] W.E. Polakowski, D.A. Cournoyer, S.K. Rogers, M.P. DeSimio, D.W. Ruck, J.W. Hoffmeister, R.A. Raines, Computer-aided breast cancer detection and diagnosis of masses using difference of Gaussians and derivative-based feature saliency, IEEE Trans. Med. Imaging 16 (6) (1997) 811–819.
[89] G.M. Brake, N. Karssemeijer, Single and multiscale detection of masses in digital mammograms, IEEE Trans. Med. Imaging 18 (7) (1999) 628–639.
[90] N. Karssemeijer, G.M. Brake, Detection of stellate distortions in mammograms, IEEE Trans. Med. Imaging 15 (5) (1996) 611–619.
[91] J.F. Canny, A computational approach to edge detection, IEEE Trans. Pattern Anal. Mach. Intel. 8 (6) (1986) 679–698.
[92] L.D. Cohen, Note on active contour models and balloons, CVGIP: Image Understanding 53 (2) (1991) 211–218.
[93] D.J. Williams, M. Shah, A fast algorithm for active contours and curvature estimation, CVGIP: Image Understanding 55 (1) (1992) 14–26.
[94] T. McInerney, D. Terzopoulos, Deformable models in medical image analysis: a survey, Med. Image Anal. 1 (2) (1996) 91–108.
[95] S. Lobregt, M.A. Viergever, A discrete dynamic contour model, IEEE Trans. Med. Imaging 14 (1) (1995) 12–24.
[96] G.M. Brake, N. Karssemeijer, J.H.C.L. Hendriks, An automatic method to discriminate malignant masses from normal tissue in digital mammograms, Phys. Med. Biol. 45 (10) (2000) 2843–2857.
[97] S. Morrison, L.M. Linnett, A model based approach to object detection in digital mammography, in: Proceedings of the IEEE International Conference on Image Processing, vol. 2, Kobe, Japan, 1999, pp. 182–186.
[98] Y. Hatanaka, T. Hara, H. Fujita, S. Kasai, T. Endo, T. Iwase, Development of an automated method for detecting mammographic masses with a partial loss of region, IEEE Trans. Med. Imaging 20 (12) (2001) 1209–1214.
[99] M. Sameti, R.K. Ward, A fuzzy segmentation algorithm for mammogram partitioning, in: K. Doi, M.L. Giger, R.M. Nishikawa, R.A. Schmidt (Eds.), Digital Mammography, Elsevier, Amsterdam, 1996, pp. 471–474.
[100] M. Sameti, R.K. Ward, B. Palcic, J. Morgan-Parkes, Texture feature extraction for tumor detection in mammographic images, 1997 IEEE Pacific Rim Conference on Comm., Computers and Signal Processing, 1997, pp. 831–834.
[101] G.L. Rogova, C. Ke, R. Acharya, P. Stomper, Feature choice for detection of cancerous masses by constrained optimization, SPIE Conference on Image Processing, vol. 3661, San Diego, CA, 1999, pp. 1440–1447.
[102] H. Li, Y. Wang, K.J.R. Liu, S.B. Lo, M.T. Freedman, Computerized radiographic mass detection C part I: lesion site selection by morphological enhancement and contextual segmentation, IEEE Trans. Med. Imaging 20 (4) (2001) 289–301.
[103] M. Sameti, R.K. Ward, J. Morgan-Parkes, B. Palcic, A method for detection of malignant masses in digitized mammograms using a fuzzy segmentation algorithm, in: Proceedings of the 19th International Conference IEEEE/MBS, 2000, pp. 513–516.
[104] D. Guliato, R.M. Rangayyan, W.A. Carnielli, J.A. Zuffo, J.E.L. Desautels, Segmentation of breast tumors in mammograms by fuzzy region growing, The IEEE Proceedings of the 20th Annual International Conference on Engineering in Medicine and Biology Society, vol. 2, 1998, pp. 1002–1005.
[105] D. Guliato, R.M. Rangayyan, W.A. Carnielli, J.A. Zuffo, J.E.L. Desautels, Detection of breast tumor boundaries using iso-intensity contours and dynamic thresholding, in: Proceedings of the Fourth International Workshop Digital Mammography, The Netherlands, 1998, pp. 253–260.
[106] B. Zheng, Y.H. Chang, D. Gur, Computerized detection of masses from digitized mammograms: comparison of single-image segmentation and bilateral-image subtraction, Assoc. Univ. Radiologists 2 (12) (1995) 1056–1061.
[107] F.F. Ying, M.L. Giger, C.J. Vyborny, K. Doi, R.A. Schmidt, Comparison of bilateral-image subtraction and single-image processing techniques in the computerized detection of mammographic masses, Invest. Radiol. (1993) 473–481.
[108] M.L. Giger, F.F. Yin, K. Doi, Y. Wu, C.J. Vyborny, R.A. Schmidt, Z. Huo, Computerized detection and characterization of mass lesions in digital mammography, 1992 IEEE International Conference on Systems, Man and Cybernetics, vol. 2, Chicago, IL, 1992, pp. 1370–1372.

[109] F.F. Yin, M.L. Giger, K. Doi, C.E. Metz, C.J. Vyborny, R.A. Schmidt, Computerized detection of masses in digital mammograms: analysis of bilateral subtraction images, Med. Phys. 18 (5) (1991) 955–963.

[110] T.K. Lau, W.F. Bischof, Automated detection of breast tumors using the asymmetry approach, Comput. Biomed. Res. 24 (1991) 273–295.

[111] A.J. Mendez, P.G. Tahoces, M.J. Lado, M. Souto, J.J. Vidal, Computer-aided diagnosis: automatic detection of malignant masses in digitized mammograms, Med. Phys. 25 (6) (1998) 957–964.

[112] A. Hadjarian, J. Bala, S.A. Gutta, S. Trachiotis, P. Pachowicz, The fusion of supervised and unsupervised techniques for segmentation of abnormal regions, in: N. Karssemeijer, M. Thijssen, J. Hendriks, L. Erning (Eds.), Digital Mammography, Kluwer, Amsterdam, 1998, pp. 299–302.

[113] L.M. Bruce, R.R. Adhami, Wavelet based feature extraction for mammographic lesion recognition, SPIE's International Symposium on Medical Imaging, CA, vol. 3304, 1997.

[114] L.M. Bruce, R. Kalluri, An analysis of the contribution of scale in mammographic mass classification, in: Proceeding of the 19th International Conference of IEEE/EMBS, 1997.

[115] L. Mann Bruce, N. Shanmugam, Using neural networks with wavelet transforms for an automated mammographic mass classifier, Proceedings of the 22nd Annual EMBS International Conference, vol. 2, 2000, pp. 985–987.

[116] P. Undrill, R. Gupta, S. Henry, M. Downing, Texture analysis and boundary refinement to outline mammography masses, in: Proceedings of the 1996 IEE Colloquium on Digital Mammography, 1996, pp. 5/1–5/6.

[117] B. Zheng, Y.H. Chang, X.H. Wang, W.F. Good, Comparison of artificial neural network and Bayesian belief network in a computer-assisted diagnosis scheme for mammography, IEEE International Conference on Neural Networks, 1999, pp. 4181–4185.

[118] H. Li, Y. Wang, K.J.R. Liu, S.B. Lo, M.T. Freedman, Computerized radiographic mass detection-part II: lesion site selection by morphological enhancement and contextual segmentation, IEEE Trans. Med. Imaging 20 (4) (2001) 302–313.

[119] B. Sahiner, H.P. Chan, N. Petrick, M.A. Helvie, M.M. Goodsitt, Design of a high-sensitivity classifier based on a genetic algorithm: application to computer-aided diagnosis, Phys. Med. Biol. 43 (10) (1998) 2853–2871.

[120] B. Zheng, Y.H. Chang, X.H. Wang, W.F. Good, D. Gur, Application of a Bayesian belief network in a computer-assisted diagnosis scheme for mass detection, SPIE Conference on Image Processing 3661 (2) (1999) 1553–1561.

[121] N.R. Mudigonda, R.M. Rangayyan, J.E. Desautels, Detection of breast masses in mammograms by density slicing and texture flow-field analysis, IEEE Trans. Med. Imaging 20 (12) (2001) 1215–1227.

[122] M. Zhang, B. Jaggi, B. Palcic, Hough spectrum and geometric texture feature analysis, Conference on Pattern Recognition, 1994—Conference B: Computer Vision & Image Processing, Proceedings of the 12th IAPR International, vol. 2, 1994, pp. 583–585.

[123] D.J. Marchette, R.A. Lorey, C.E. Priebe, An analysis of local feature extraction in digital mammography, Pattern Recognition 30 (9) (1997) 1547–1554.

[124] Z.M. Huo, M.L. Giger, C.J. Vyborny, D.E. Wolverton, R.A. Schmidt, K. Doi, Automated computerized classification of malignant and benign masses on digitized mammograms, Acad. Radiol. 5 (1998) 155–168.

[125] A.S. Constantinidis, M.C. Fairhurst, A.F.R. Rahman, A new multi-expert decision combination algorithm and its application to the detection of circumscribed masses in digital mammograms, Pattern Recognition 34 (8) (2001) 1527–1537.

[126] S.O. Belkasim, M. Shridhar, M. Ahmadi, Pattern recognition with moment invariants: a comparative study and new results, Pattern Recognition 24 (12) (1991) 1117–1138.

[127] A.S. Constantinidis, M.C. Fairhurst, A.F.R. Rahman, Detection of circumscribed masses in digital mammograms using behavior–knowledge space method, Electron. Lett. 36 (4) (2000).

[128] K. Bovis, S. Singh, Detection of masses in mammograms using texture features, in: Proceedings of the 15th International Conference on Pattern Recognition, 2000, pp. 267–269.

[129] L. Tarassenko, P. Hayton, N. Cerneaz, M. Brady, Novelty detection for the identification of masses in mammograms, Fourth International Conference on Artificial Neural Networks, 1995, pp. 442–447.

[130] B. Sahiner, H.P. Chan, N. Petrick, M.A. Helvie, M.M. Goodsitt, Computerized characterization of masses on mammograms: the rubber band straightening transform and texture analysis, Med. Phys. 25 (4) (1998) 516–526.

[131] B. Sahiner, H.P. Chan, N. Petrick, M.A. Helvie, L.M. Hadjiiski, Improvement of mammographic mass characterization using spiculation measures and morphological features, Med. Phys. 28 (7) (2001) 1455–1465.

[132] M.K. Hu, Visual pattern recognition by moments invariants, IRE Trans. Inf. Theory IT-8 (1962) 179–187.

[133] N.R. Mudigonda, R.M. Rangayyan, J.L. Desautels, Gradient and texture analysis for the classification of mammographic masses, IEEE Trans. Med. Imaging 19 (10) (2000) 1032–1043.

[134] L.M. Bruce, R.R. Adhami, Classifying mammographic mass shapes using the wavelet transform modulus-maxima method, IEEE Trans. Med. Imaging 18 (1999) 1170–1177.

[135] J. Kilday, F. Palmieri, M.D. Fox, Classifying mammographic lesions using computer-aided image analysis, IEEE Trans. Med. Imaging 12 (4) (1993) 664–669.

[136] Z. Huo, M.L. Giger, C.J. Vyborny, Computerized analysis of multiple-mammographic views: potential usefulness of special view mammograms in computer-aided diagnosis, IEEE Trans. Med. Imaging 20 (12) (2001).

[137] Z. Huo, M.L. Giger, C.J. Vybomy, U. Bick, P. Lu, D.E. Wolverton, R.A. Schmidt, Analysis of speculation in the computerized classification of mammographic masses, Med. Phys. 22 (1995) 1569–1579.

[138] N.M. El-Faramawy, R.M. Rangayyan, J.E.L. Desautels, O.A. Alim, Shape factors for analysis of breast tumors in mammograms, 1996 Canadian Conference on Electrical and Computer Engineering, 1996, pp. 355–358.

[139] S. Baeg, N. Kehtarnavaz, E.R. Dougherty, Morphological texture based classification of abnormalities in mammograms, Int. Soc. Opt. Eng. 3661 (1999) 1208–1218.

[140] D. Wei, H.P. Chan, M.A. Helvie, B. Sahiner, N. Petrick, D.D. Adler, M.M. Goodsitt, Multiresolution texture analysis for classification of mass and normal breast tissue on digital mammograms, Int. Soc. Opt. Eng. 2434 (1995) 606–611.

[141] R.M. Rangayyan, N.M. Faramawy, J.E. Desautels, O.A. Alim, Measures of acutance and shape for classification of breast tumors, IEEE Trans. Med. Imaging 16 (6) (1997).

[142] M.A. Kupinski, M.L. Giger, Investigation of regularized neural networks for the computerized detection of mass lesions in digital mammograms, in: Proceeding of the 19th International Conference of IEEE/EMBS, 1997.

[143] D. Wei, H.P. Chan, N. Petrick, B. Sahiner, M.A. Helvie, D.D. Adler, M.M. Goodsitt, False-positive reduction technique for detection of masses on digital mammograms: global and local multiresolution texture analysis, Med. Phys. 24 (6) (1997) 903–914.

[144] S.N.C. Cheng, H.P. Chan, M.A. Helvie, M.M. Goodsitt, D.D. Adler, D.C.St. Clair, Classification of mass and non-mass regions on mammograms using artificial neural networks, J. Imaging Sci. Technol. 38 (6) (1994).

[145] R.M. Haralick, H.K. Shanmugam, I. Dinstein, Texture features for image classification, IEEE Trans. Systems, Man, Cybernet. SMC-3 (6) (1973) 610–621.
[146] A. Petrosia, H.P. Chan, M.A. Helvie, M.M. Goodsitt, D.D. Adler, Computer-aided diagnosis in mammography: classification of mass and normal tissue by texture analysis, Phys. Med. Biol. 39 (1994) 2273–2288.
[147] B. Sahiner, H.P. Chan, N. Petrick, D. Wei, M.A. Helvie, D.D. Adler, M.M. Goodsitt, Classification of mass and normal breast tissue: a convolution neural network classifier with spatial domain and texture images, IEEE Trans. Med. Imaging 15 (5) (1996) 598–609.
[148] J.S. Weszka, C.R. Dyer, A. Rosenfeld, A comparative study of texture measures for terrain classification, IEEE Trans. Systems, Man, Cybernet. SMC-6 (4) (1976) 269–285.
[149] M.M. Galloway, Texture classification using gray level run length, Comput. Graphics Image Process. 4 (1975) 172–179.
[150] M.L. Giger, Z. Huo, M.A. Kupinski, C.J. Vyborny, Computer-aided diagnosis in mammography, in: M. Sonka, J.M. Fitzpatrick (Eds.), Handbook of Medical Imaging, vol. 2, SPIE Press, 2000, pp. 915–1004.
[151] D. Wei, H.P. Chan, M.A. Helvie, B. Sahiner, N. Petrick, D.D. Adler, M.M. Goodsitt, Classification of mass and normal breast tissue on digital mammograms: multiresolution texture analysis, Phys. Med. 22 (9) (1995) 1501–1513.
[152] M.A. Kupinski, M.L. Giger, Feature selection and classifiers for the computerized detection of mass lesions in digital mammography, IEEE International Conference on Neural Networks, 1997, pp. 2460–2463.
[153] L. Hadjiiski, B. Sahiner, H.P. Chan, N. Petrick, M. Helvie, Classification of malignant and benign masses based on hybrid ART2LDA approach, IEEE Trans. Med. Imaging 18 (12) (1999) 1178–1186.
[154] L. Hadjiiski, B. Sahiner, H.P. Chan, N. Petrick, M. Helvie, Hybrid unsupervised-supervised approach for computerized classification of malignant and benign masses on mammograms, SPIE Conference on Image Processing, vol. 3661, 1999.
[155] H.P. Chan, D. Wei, M.A. Helvie, B. Sahiner, D.D. Adler, M.M. Goodsitt, N. Petrick, Computer-aided classification of mammographic masses and normal tissue: linear discriminant analysis in texture feature space, Phys. Med. Biol. 40 (1995) 857–876.
[156] M.M. Tatsuoka, Multivariate Analysis, Techniques for Educational and Psychological Research, Macmillan, New York, 1988.
[157] B. Zheng, Y.H. Chang, X.H. Wang, W.F. Good, D. Gur, Feature selection for computerized mass detection in digitized mammograms by using a genetic algorithm, Acad. Radiol. 6 (1999) 327–332.
[158] D. Wei, B. Sahiner, H.P. Chan, N. Petrick, Detection of masses on mammograms using a convolution neural network, IEEE International Conference on Acoustics, Speech & Signal Processing, 1995, pp. 3483–3486.
[159] W.F. Good, B. Zheng, Y.H. Chang, X.H. Wang, D. Gur, Multi-image CAD employing features derived from ipsilateral mammographic views, SPIE Conference on Image Processing, vol. 3661, 1999, pp. 474–485.
[160] H.D. Cheng, M. Cui, Mass lesion detection with a fuzzy neural network, Pattern Recognition 37 (6) (2004) 1189–1200.
[161] R.O. Duda, P.E. Hart, D.G. Stork, Pattern Classification, second ed., Wiley, New York, 2001.
[162] P.A. Lachenbruch, Discriminant Analysis, Hafner, New York, 1975.
[163] S. Baeg, N. Kehtarnavaz, Texture based classification of mass abnormalities in mammograms, in: Proceedings of the IEEE Symposium on Computer-based Medical Systems, 2000, pp. 163–168.
[164] R.P. Velthuizen, J.I. Gaviria, Computerized mammographic lesion description, in: Proceedings of the First Joint BMES/EMBS Conference, 1999, p. 1034.
[165] D.B. Fogel, E.C. Wasson III, E.M. Boughton, Evolving artificial neural networks for screening features from mammograms, Artif. Intell. Med. 14 (1998) 317–326.
[166] C.E. Floyd, J.Y. Lo, A.J. Yun, D.C. Sullivan, P.J. Kornguth, Prediction of breast cancer malignancy using an artificial neural network, Cancer 74 (11) (1994) 2944–2948.
[167] F.V. Jensen, An Introduction to Bayesian Network, Springer, New York, NY, 1996.
[168] M. Schmitt, J. Mattioli, Measures morphologiques, Morphologie Mathematique, Masson, Paris, 1994.
[169] A.K. Jain, R.P.W. Duin, J. Mao, Statistical pattern recognition: a review, IEEE Trans. Pattern Anal. Mach. Intel. 22 (1) (2000) 4–37.
[170] L. Bocchi, G. Coppini, J. Nori, G. Valli, Detection of single and clustered microcalcifications in mammograms using fractals models and neural networks, Med. Eng. Phys. 26 (2004) 303–312.
[171] L. Xu, A. Krzyzak, C.Y. Suen, Methods of combining multiple classifiers and their applications to handwriting recognition, IEEE Trans. Systems, Man, Cybernet. 22 (3) (1992) 418–435.
[172] G.A. Carpenter, S. Grossberg, ART2: self-organization of stable category recognition codes for analog input patterns, Appl. Opt. 26 (23) (1987) 4919–4930.
[173] G.A. Carpenter, S. Grossberg, D.B. Rosen, ART2-A: an adaptive resonance algorithm for rapid category learning and recognition, Neural Networks 4 (4) (1991) 493–504.
[174] Z. You, A.K. Jain, Performance evaluation of shape matching via chord length distribution, Comput. Vision, Graphics, Image Process. 28 (1984) 185–198.
[175] R.M. Mishikara, Mapmmographic databases, Breast Dis. 10 (1998) 137–150.
[176] K. Woods, M.Y. Sallam, K.W. Bowyer, Evaluating Detection Algorithms, in: N. Karssemeijer, M. Thijssen, J. Hendriks, L. Erning (Eds.), Digital Mammography, Kluwer, Amsterdam, 1998, pp. 19–45.
[177] J.A. Swets, ROC analysis applied to the evaluation of medical imaging techniques, Invest. Radiol. 14 (2) (1979) 109–121.
[178] C.E. Metz, ROC methodology in radiological imaging, Invest. Radiol. 21 (1986) 720–733.
[179] H.D. Cheng, X.J. Shi, A simple and effective histogram equalization approach to image enhancement, Digital Signal Process. 14 (2) (2004) 158–170.
[180] A. Wald, Statistical Decision Functions, Wiley, New York, 1950.
[181] L.B. Lusted, Introduction to Medical Decision Making, Thomas, Springfield, IL, 1968.
[182] L.B. Lusted, Decision-making studies in patient management, N. Engl. J. Med. 284 (1971) 416–424.
[183] L.B. Lusted, Signal detectability and medical decision-making, Sci. 171 (1971) 1217–1219.
[184] C. E. Metz, P. L. Wang, H. B. Kronman, A new approach for testing the significance of differences between ROC curves measured from correlated data, in: Proceedings of the Information Processing in Medical Imaging, Nijhoff, Amsterdam, 1984, pp. 432–445.
[185] J.P. Egan, G.Z. Greenberg, A.I. Schulman, Operating characteristics, signal detectability, and the method of free response, J. Acoust. Soc. Am. 33 (1961) 993–1007.
[186] P.C. Bunch, J.F. Hamilton, G.K. Sanderson, A.H. Simmons, A free-response approach to the measurement and characterization of radiographic observer performance, J. Appl. Photogr. Eng. 4 (1978) 166–171.
[187] D.P. Chakraborty, Free-response methodology: alternate analysis and a new observer performance experiment, Radiology 174 (1990) 873–881.
[188] D.D. Dorfman, E. Alf Jr., Maximum-likelihood estimation of parameters of signal detection theory and determination of confidence intervals: rating method data, J. Math. Psychol. 6 (1969) 487–496.
[189] L. Li, W. Qian, L.P. Clarke, Digital mammography: directional wavelet analysis for feature extraction and mass detection, Acad. Radiol. 4 (11) (1997) 724–731.

[190] Bin Zheng, Y.H. Chang, D. Gur, Computerized detection of masses from digitized mammograms using single image segmentation and multi-layer topographic feature analysis, Acad. Radiol. 2 (1995) 959–966.
[191] F.F. Yin, M.L. Giger, K. Doi, C.J. Vyborny, R.A. Schmidt, Computerized detection of masses in digital mammograms: automated alignment of breast images and its effect on bilateral-subtraction technique, Med. Phys. 21 (1994) 445–452.
[192] F.F. Yin, M.L. Giger, K. Doi, C.J. Vyborny, R.A. Schmidt, Computerized detection of masses in digital mammograms: investigation of feature-analysis techniques, J. Digital Imaging 7 (1994) 18–26.
[193] M. Kupinski, M. L. Giger, P. Lu, Z. Huo, Computerized detection of mammographic lesions: performance of an artificial neural network with enhanced feature extraction, in: Proceedings of SPIE, 1995, pp. 598–560.
[194] J. Besag, On the statistical analysis of dirty pictures, J. R. Stat. Soc. Ser. B 48 (3) (1986) 259–302.
[195] P. Skaane, E.M. Sager, J.B. Olsen, M. Abdelnoor, A. Berger, P.A. Wolff, G. Kullmann, Diagnostic value of ultrasonography in patients with palpable mammographically noncalcified breast tumors, Acta Radiol. 40 (2) (1999) 163–168.
[196] W.T. Yang, M. Suen, N.U.I. Bao, Sonographic features of benign papillary neoplasms of the breast: review of 22 patients, J. Ultrasound Med. 16 (1997) 161–168.
[197] R.L. Webber, H.R. Underhill, R.I. Freimanis, A controlled evaluation of tuned-aperture computer tomography applied to digital spot mammography, J. Digital Imaging 13 (2000) 90–97.
[198] H.D. Cheng, X.P. Cai, X.W. Chen, L.M. Hu, X.L. Lou, Computer-aided detection and classification of microcalcifications in mammograms: a survey, Pattern Recognition 36 (2003) 2967–2991.
[199] S. Osher, R.P. Fedkiw, Level set methods: an overview and some recent results, J. Comput. Phys. 169 (2001) 463–502.
[200] A. Tsai, A. Yezzi, W. Wells, C. Tempany, D. Tucker, A. Fan, W.E. Grimson, A. Willsky, A shape-based approach to the segmentation of medical imagery using level sets, IEEE Trans. Med. Imaging 22 (2) (2003) 137–154.
[201] W.J. Niessen, B.M. Romeny, M.A. Viergever, Geodesic deformable models for medical image analysis, IEEE Trans. Med. Imaging 17 (4) (1998) 634–641.
[202] D. Terzopoulos, A. Witkin, M. Kass, Constraints on deformable models: recovering 3-D shape and nonrigid motion, Artif. Intell. 36 (1988) 91–123.
[203] B. Zheng, Y.H. Chang, W.F. Good, D. Gur, Performance gain in computer-assisted detection schemes by averaging scores generated from artificial neural networks with adaptive filtering, Med. Phys. 28 (2001) 2302–2308.
[204] L.H. Li, Y. Zheng, L. Zhang, R.A. Clark, False-positive reduction in CAD mass detection using a competitive classification strategy, Med. Phys. 28 (2001) 250–258.
[205] P. Sajda, C. Spence, J. Pearson, Learning contextual relationships in mammograms using a hierarchical pyramid neural network, IEEE Trans. Med. Imaging 21 (2002) 239–250.
[206] S.C.B. Lo, H. Li, Y. Wang, L. Kinnard, M.T. Freedman, A multiple circular path convolution neural network system for detection of mammographic masses, IEEE Trans. Med. Imaging 21 (2002) 150–158.
[207] G.D. Tourassi, Rene Vargas-Voracek, Computer-assisted detection of mammographic masses: a template matching scheme based on mutual information, Med. Phys. 30 (2003) 2123–2130.

About the Author—HENG-DA CHENG received his Ph.D. in Electrical Engineering from Purdue University, West Lafayette, IN, in 1985 (supervisor: K. S. Fu). Currently, he is a Full Professor, Department of Computer Science, and Adjunct Full Professor, Department of Electrical and Computer Engineering, Utah State University. Dr. Cheng is an Adjunct Professor and Doctorial Supervisor of Harbin Institute of Technology (HIT), an Adjunct Professor of Harbin Engineering University, and a Guest professor of Remote Sensing Application Institute, Chinese Academy of Sciences, a Guest professor of Wuhan University, a Guest professor of Shantou University and a Visiting professor of Beijing Jiaotung University.
Dr. Cheng has published more than 200 technical papers, is the co-editor of the book, Pattern Recognition: Algorithms, Architectures and Applications, and the editor of four conference proceedings. His research interests include: Artificial Intelligence, Computer Vision, Pattern Recognition & Image Processing, Medical Information Processing, Fuzzy Logic, Neural Networks and Genetic Algorithms, Parallel Processing, Parallel Algorithms, and VLSI algorithms and architectures.
Dr. Cheng is the General Chairman of JCIS 2005 (Joint Conference of Information Sciences) and the General Chair and Program Chair, the Sixth International Conference on Computer Vision, Pattern Recognition & Image Processing (CVPRIP2005), was the Fifth International Conference on Computer Vision, Pattern Recognition & Image Processing (CVPRIP2003), the Fourth International Conference on Computer Vision, Pattern Recognition & Image Processing (CVPRIP2002), the Third International Conference on Computer Vision, Pattern Recognition & Image Processing (CVPRIP2000), and the First International Workshop on Computer Vision, Pattern Recognition & Image Processing (CVPRIP98), and the Program Co-Chair of Vision Interface '90, 1990. He served as a program committee member and session chair for many conferences, and as a reviewer for many scientific journals and conferences. Dr. Cheng has been listed Who's Who in the World, Who's Who in America, Who's Who in Communications and Media, Who's Who in Science and Engineering, Who's Who in Finance and Industry, Men of Achievement, 2000 Notable American Men, International Leaders in Achievement, Five Hundred Leaders of Influence, International Dictionary of Distinguished Leadership, etc. He has been appointed as Member of the International Biographical Center Advisory Council, The International Biographical Center, England. And a Member of the Board of Advisors, the American Biographical Institute, USA. Dr Cheng is a Senior Member of IEEE society, and a Member of the Association of Computing Machinery. Dr. Cheng is also an Associate Editor of Pattern Recognition and an Associate Editor of Information Sciences.

About the Author—XIANGJUN SHI received his B.S. degree in Computational Mathematics and Computer Application from the Department of Computer Science and Engineering, Hangzhou University, China in 1986, and the M.E. degree in Computer Graphics from the Department of Computer Science and Engineering, Zhengjian University, China in 1989. From 1989 to 1998, he was an Assistant Professor in Hangzhou University (1989–1995) and Shantou University (1995–1998). From 1998 to 2000, he was an Associate Professor in Shantou University. Since 2001, he is a Ph.D. student in the Department of Computer Science, Utah State University. His research interests include: Computer Vision, Pattern Recognition, Image Processing and Artificial Intelligence.

About the Author—RUI MIN received his B.S. degree in Management Information System (1995) from Dalian Maritime University, China and M.S. degree in Computer Science (2003) from Utah State University. He worked in Liaoning MEC Group Co., Ltd as a software and networking engineer from 1995 to 2000. Currently, he is a Ph. D. student in Computer Science Department, Utah State University. His research areas include Computer Vision, Pattern Recognition and Image Processing.

About the Author—LIMING HU received his Bachelor of Science degree from the Department of Computer Science, in 1995, and the Master of Computer Engineering degree from the Institute of Machine Intelligence, Nankai University, China, in 1998. From 1998 to 2001, he was a software Engineer working on Telecom software development at Shanghai Bell, Inc. Now he is a Ph.D. candidate of the Department of Computer Science, Utah State University. His research interests are in Pattern Recognition, Image Processing and Artificial Intelligence.

About the Author—XIAOPENG CAI received his bachelor of science degree from Mathematics Department, Shandong University and master of science degree from Computer Science Department, Utah State University, in 1999 and 2004, respectively. His research interests are image and signal processing, fuzzy logic, and software engineering.

About the Author—HAINING DU received his B.S. degree in 1998, and M.S. degree in 2001, from Control Theory and Control Engineering Department in Southeast University, China, and M.S. degree in 2004 from Computer Science Department, Utah State University, U.S.A. His research interests are in the areas of Computer Vision, Pattern Recognition and Image Processing.